2004

Investigation of Characteristics of Bounded Wall Jets in Dead End Mine Headings

Lavanya Rangubhotla
University of Kentucky, rsllavanya@gmail.com

ABSTRACT OF THESIS

Investigation of Characteristics of Bounded Wall Jets in Dead End Mine Headings

A comprehensive experimental study has been conducted using Particle Image Velocimetry (PIV) for a wide array of ventilation schemes and mining configurations for the purpose of examining ventilation characteristics in dead end mine headings. Flow behaviors in two basic mining sequences of box and slab cuts for 30 ft and 60 ft deep cuts were studied. The present thesis discusses the effect for various geometric and flow parameters including the variation of inlet flow velocities, entry heights, face zone widths and curtain widths on the flow behavior. The Reynolds number Re considered for this study ranges from $1 \cdot 10^5$ to $3 \cdot 10^6$ based on curtain width and exit velocity. The variation of the face zone and the curtain widths considerably affected the flow behavior, resulting in recirculation regions in the face area for critical combinations. Jet spreading angles and virtual origins have been calculated for the different geometries showing that an optimum range of face and curtain widths exists. A detailed discussion employing various scenarios for exhaust ventilation systems has also been made. Full-size measurements and comparison of the experimental data with numerical simulations is presented. Implementation of machine-mounted scrubbers in the blowing system are discussed for different values of the ventilation ratios (Q_s/Q_{in}) ranging from 14% to 53%. The scrubber system, typically introduced for dust collection, is also shown to be a useful tool in providing adequate ventilation to the immediate face area.

Keywords: Mine Ventilation, Flow Separation, Mining Scenarios, Wall Bounded Jets, Scrubber Ventilation System.

Lavanya Rangubhotla

12/14/04

Investigation of Characteristics of Bounded Wall Jets in Dead End Mine Headings

By

Lavanya Rangubhotla

Jamey D. Jacob
(Director of Thesis)

George Huang
(Director of Graduate Studies)

December 15, 2004
(Date)

RULES FOR THE USE OF THESIS

Unpublished Thesis submitted for the Doctor's degree and deposited in the University of Kentucky Library are as a rule open for inspection, but are to be used only with due regard to the rights of the authors. Bibliographical references may be noted, but quotations or summaries of parts may be published only with the permission of the author, and with the usual scholarly acknowledgments.

Extensive copying or publication of the thesis in whole or in part requires also the consent of the Dean of The Graduate School of the University of Kentucky.

THESIS

Lavanya Rangubhotla

The Graduate School
University of Kentucky
2004

Investigation of Characteristics of Bounded Wall Jets in Dead End Mine Headings

---

THESIS

A thesis submitted in partial fulfillment of the
requirements for the degree of Master of Science
in Mechanical Engineering in the College of Engineering
at the University of Kentucky.

By

Lavanya Rangubhotla

Lexington, Kentucky

Director: Dr. Jamey D. Jacob, Dr. Andrzej M. Wala

University of Kentucky, Lexington, Kentucky

2004

Acknowledgements

First and foremost, I would offer a very special thanks to my parents Mr. and Mrs. Sastry Rangubhotla, my brother and his lovely family Mr and Mrs. Krishna Rangubhotla, Vaishnavi and Sindu and my very good friend Vijayram Vissapragada, for their understanding and support throughout my Masters. They have been very supportive both morally and mentally right from the day one, and have constantly given me more reasons and opportunities to flourish in my career.

I had an immense pleasure in working with both of my advisors Dr. Jamey D.Jacob and Dr . Andrezj M. Wala. Both of them who are greatly talented, experienced and highly knowledgeable teachers helped me both acadamically and personally. Under their tutelege, my knowledge grew in leaps and bounds. Their adivice and support have contributed a major part for my completing my Masters thesis.

Also I would like to offer thanks all my teachers who were helpful in building a castle of knowledge about the various topics in Fluid Dynamics. I offer special thanks to Dr. Vincent Capece, who was helpful not only acadamically but also professionally assisting in my job hunt.

Finally I am thankful to all my friends and people from the Fluid Mechanics Lab for their constant support.

Table of Contents

List of Figures

List of Tables

Chapter 1

Background and Introduction

1.1 Background

Since the advent of remote controlled continuous miners and extended cuts for room and pillar mining operations (Wellman, 1981), the efficiency and productivity of mining operations has increased significantly. However, this high production presents environmental problems such as the accumulation of coal dust and higher levels of methane at the face during coal extraction. During coal extraction, the concentration of methane released, if it exceeds a certain limit, will result in underground explosions. To reduce this risk, the methane should be diluted with outside air delivered into the face area. Various ventilation techniques such as machine-mounted scrubber systems, extendable line curtains, jet fans or a combination of these have been used by the mining industry to achieve this result. One of the most prominent ventilation techniques used in conjunction with these modern mining systems (Goodman et al., 1990) is the blowing curtain with a machine-mounted dust scrubber. Implementation of this technique has a significant influence on the airflow patterns in the entry working area and the design of air handling capacities. The major goal of this research is to study and understand the complexity of such behaviors using Particle Image Velocimetry (PIV).

The former U.S. Bureau of Mines (currently NIOSH), Mine Safety and Health Administration, and the coal industry have conducted significant studies to evaluate the performances of face ventilation systems through the use of full scale tests (underground/surface) or scaled physical modeling. These studies led to recommendations that make these systems more effective. However, because of the aerodynamic complexity in the face area due to the variety of ventilation arrangements and the limitations of the experimental methods, some doubts still exist when evaluating the effectiveness of such a system.

As mentioned before, since remote controlled continuous miners were introduced, deep cut mining presented an opportunity for mine operators to increase productivity. However, the presence of airborne coal dust in the face area was a major obstruction. This coal dust can cause poor visibility around the cutting head and can expose the miners to high levels of respirable dust. A practical means of removing this dust is the dust-collecting scrubber mounted directly on the mining machine (U.S. Bureau of Mines, 1980). When the scrubbers were added to the face ventilation system of coal mines, the existing arrangements of the face ventilation system were altered to accommodate these scrubbers.

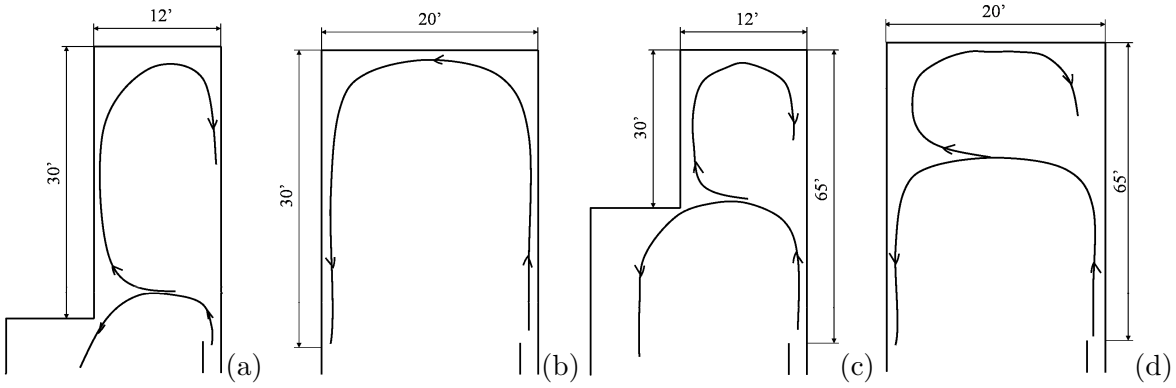

Figure 1.1: Flow patterns for 30 ft deep cut with and without the slab; figures (a) and (b) and Flow patterns for a 60 ft deep cut with and without the slab; figures (c) and (d). Note that the scaling changes between figures (b) and (c).

Many studies concerning the face ventilation with scrubbers were carried out in United States in the last twenty years, including Gillies (1982), Clouse (1982), Thimons et al. (1999). Most of the researchers, followed the Luxner comments (1969) concerning the higher effectiveness of the blowing system versus the exhaust system, recommended the blowing system as the best suited ventilation systems for scrubber applications, particularly because the free jet of high initial momentum leaving the end of the line curtain should penetrate into the immediate face area sweep the face and flow into the return. This is true according to Figures 1.2b, as long as the entry width is more than 16 foot, as was discovered during this study (Wala et al., 2001). This means that only during the slab cutting scenario does the advantage of the blowing curtain prevail. For the rest of the mining scenarios the ventilation air does not flow to the immediate face area where it is mostly needed in gassy mines for methane dilution. Results showing these behaviors are presented in Chapter 3.

The effects of machine-mounted scrubber systems on levels of methane and respirable dust were tested first by Ingersoll Rand Research Inc. (Clouse, 1982). These studies have shown that

properly designed machine-mounted scrubber systems can allow curtain setbacks of 12.2 m (40 ft), while still controlling respirable dust and methane levels. At that time, it was shown that the application of the machine-mounted scrubber primarily helped to collect respirable dust at the face (dust source location) and improved the visibility. The experiments were performed for different ventilation ratios $\boldsymbol{Q_s/Q_{in}}$), where $\boldsymbol{Q_s}$ and $\boldsymbol{Q_{in}}$ are the scrubber flow rate and curtain inlet flow rate, respectively. Based on the Ingersoll-Rand studies, MSHA recommended a ratio between the scrubber flow $\boldsymbol{Q_s}$ and the intake flow $\boldsymbol{Q_{in}}$ of close to one. A study performed by Jayaraman (1992), supports these finding, however, latest studies performed by Taylor et al., (1996) and by Thimons et al., (1999) show that the relations between face ventilation performance and scrubber/ventilation flow ratios are more complicated (recirculation etc) than was previously thought.

Blowing face ventilation systems with scrubber-equipped continuous mining machines are commonly used in U.S. underground coal-mines for extended cuts. This type of face ventilation system has been shown to be the most efficient if all the components of the system are working properly. However, in cases of scrubber failure or use of a continuous mining machine without scrubber or other mechanical face ventilation enhancing devices, the recommended blowing ventilation system must be replaced by an exhaust system. These face ventilation systems must be designed by the mining industry and have to be submitted to MSHA for approval. A tool must be developed to help the design and the approval process of these face ventilation systems. However, results of numerical simulations need to be validated with experimental data.

1.2 Introduction

The goal of this thesis is to understand the complex flow behaviors in the face area for various mining scenarios and to understand the effects and the results of various parameters affecting the flow. To study this behavior, a scaled physical model was previously designed and built of plexiglas for the selected face ventilation system as shown in Figure 1.1 (Wala et al., 2000). Then a series of measurements using Particle Image Velocimetry (PIV) (Turner et al., 2002) were performed, to determine the velocity fields in the model. Study concerning the effect of various geometric and flow parameters on the air flow behaviors were previously performed and discussed (Wala et al., 2002). Continuation of this parametric study was carried out as a part of this thesis. The experimental data using the scaled physical model was used for the validation of CFD simulations (Wala et al., 2003 and 2004). The detailed discussion about the experimental setup is mentioned in Chapter 2.

The face ventilation plan shown in Figure 1.2 is considered as the basis for deep cut mining with blowing curtain in this current study. As can be seen from Figure 1.1, the air is carried into

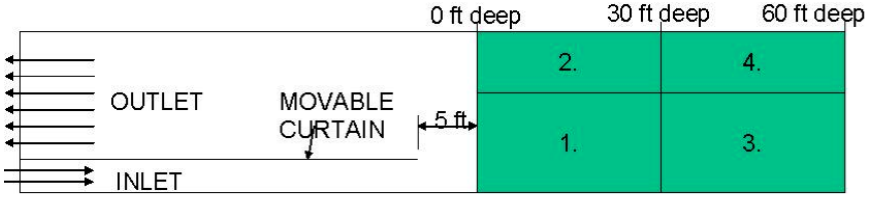

Figure 1.2: Test section geometry.

the face area through the inlet blowing curtain and is taken out by the wide part of the opening. The mining sequences follow the order numbered in the figure. The goal of the study was to understand the complex flow behavior in the face area. The important characteristic of the flow pattern as discussed by Wala et al., 2000 and 2001, specifically for the box cutting sequences 1 and 3 as in Figure 1.1, was that 70% to 80% of the air leaving the end of the blowing curtain almost immediately separates from the rib (wall) and turns back towards the return. This behavior can be seen in Figures 1.1a and 1.1c. The rest of the curtain airflow, approximately 20% to 30%,called the secondary flow, continues to flow towards the immediate face area in the opposite direction. As can be seen in general, the ventilation air delivered by the blowing curtain does not flow into the immediate face area.

Experiments were conducted for different scenarios with different combinations of parameters such as curtain setback, intake air quantity delivered by the curtain, tight-rib distance (curtain distance from the rib), and mining sequence. The data collected during these studies allows direct conclusions concerning the flow behavior. The results for the above discussed studies can be seen in Chapter 3.

From the studies discussed in Chapter 3, it was observed that some of the parameters were unable to bring air to the face area primarily for the box cutting sequences (effect of variation of width of the face zone). Therefore, the effect of a scrubber system on face ventilation was studied and the results are discussed in Chapter 4. However, in some situations where the miner machine is not equipped with the scrubber, the exhaust ventilation system is prefered. The results discussing the flow behaviors for various scenarios utilizing the exhaust system are discussed in Chapter 5.

It was presumed that during the initial studies performed in the 1980's and 1990's for the full-scale measurements, the flow patterns for these mining scenarios was not fully understood because of limited opportunity to monitor the flow patterns. The only sources of information concerning the similar flow behaviors as shown in Figure 1.2 were recognized and described by Luxner (1969) and Taylor et al., (1997). As this unsteady flow behavior (flow separation from the

wall) was so predominant, full-scale measurements were needed to validate this flow behavior. To ensure that scaled model test results interpret conditions reliably in the underground face area the cooperative validation testing has been performed using full-scale testing gallery at the NIOSH Research Center. These studies proved that a 1:15 scaled laboratory model used for the project is a valid tool and realistically simulated underground conditions for the face ventilation systems. Observations showed that the flow patterns for one of the scenarios tested using the laboratory scaled model and the full-scale model are similar. These results can be seen in Chapter 6. Chapter 7 draws the final conclusions and discussion for the study performed and suggests directions for future work.

Chapter 2

Experimental Arrangement

2.1 Introduction

Conducting experimental studies in a coal mine and full-size testing galleries is very expensive and time consuming. A better way to study such flow behavior is using a scaled model which is cost effective, simple in construction, easy to perform and flexible. So for these reasons a 1:15 scaled physical model was designed and constructed for the experiments. This physical model was simple in its construction and also very flexible so as to have different arrangements for various ventilating scenarios with less cost and effort. As the flow is unsteady, PIV (Particle Image Velocimetry) was considered which provides instantaneous realizations of the flow field. Numerical simulations can also be used to study such behavior but they need experimental data for their validation.

2.2 Scaled Physical Models

2.2.1 Models for the Face Ventilation System

The analysis of face airflow patterns was undertaken using 1:15 physically scaled model. This scaled model of a typical underground room and pillar coal mine with an entry of 140 mm (corresponding to 2.1 m (7 ft) in a full-scale model) high and 407 mm (corresponding to 6.1 m (20 ft) in a full-scale model) wide was designed and built out of optically transparent Plexiglas as shown in Figure 2.1. The four basic arrangements are shown in Figure 2.2. Figure 2.2a and b represent the scaled models for 30 ft deep cuts with and without the slabs respectively. Figure 2.2c and d represent the scaled models for 60 ft deep cuts with and without the slab, respectively. Scaling of the entry flow rate was performed using dimensional analysis based on the Reynolds number,

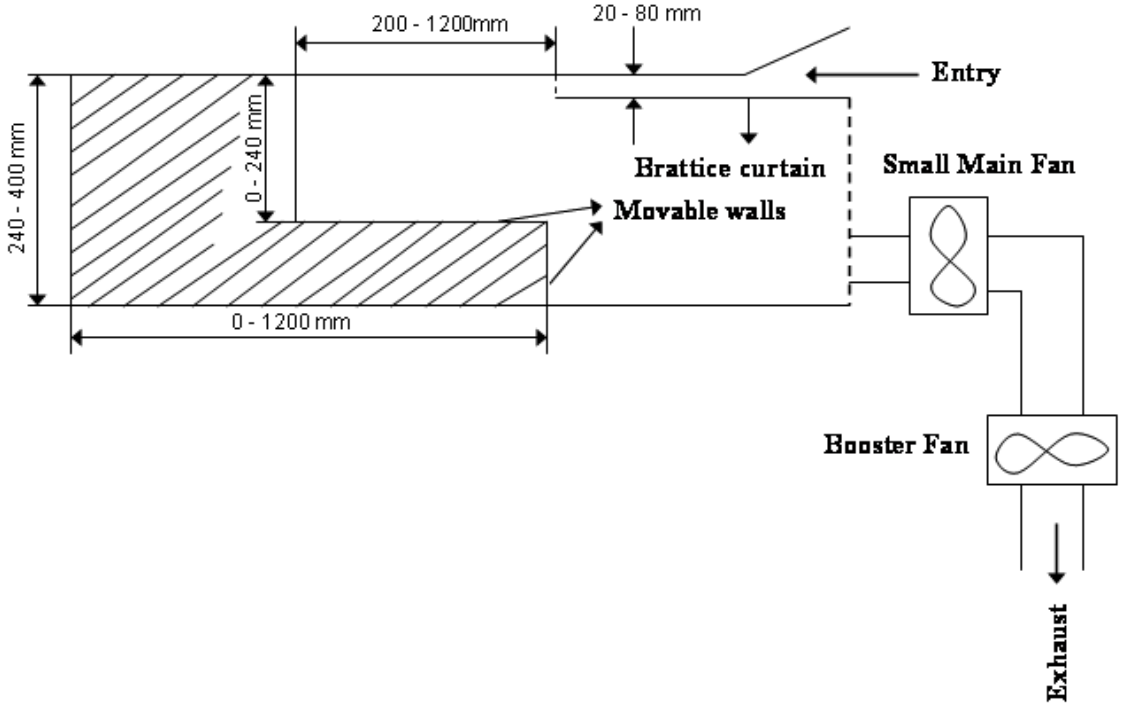

Figure 2.1: Schematic of the scaled physical model

$Re = UL/\nu$, where U and L are the velocity at the brattice line mouth and width of the inflow (distance between brattice line and entry rib), respectively. The Re range considered for this study were from 10^5 to 3x10^6. The working area, from the end of the curtain to the face area, where movable Plexiglas walls are used to replicate many different ventilation configurations such as box-cut or slab-cut arrangements with brattice setback distances varying from zero to 120 mm, corresponding to 18.3 m (60 ft) in a full-scale model. The middle section consisting of an ordinary mining entry with a partition (brattice line/curtain), divides the entry into a narrow 40 mm, (corresponding to 0.6 m (2 ft) in a full-scale model) wide intake and an 367 mm (corresponding to 5.5 m (18 ft) in a full-scale model) wide return airways. The return section has a small main fan and a booster fan which are used for both driving the flow and removing the dust (seeding in a scaled model) outside the system. Both fans were needed to obtain the required flow rate. By changing the fan location, either blowing or exhaust ventilation systems can be attained. The primary airflow through the entry was drawn by a main axial fan in series with a smaller axial speed controllable auxiliary fan. The maximum available airflow induced through the model corresponds to 0.2 m^3/s (430 cfm) (corresponding to 3.0 m^3/s (6,500 cfm) in a full-scale model) for underground conditions.

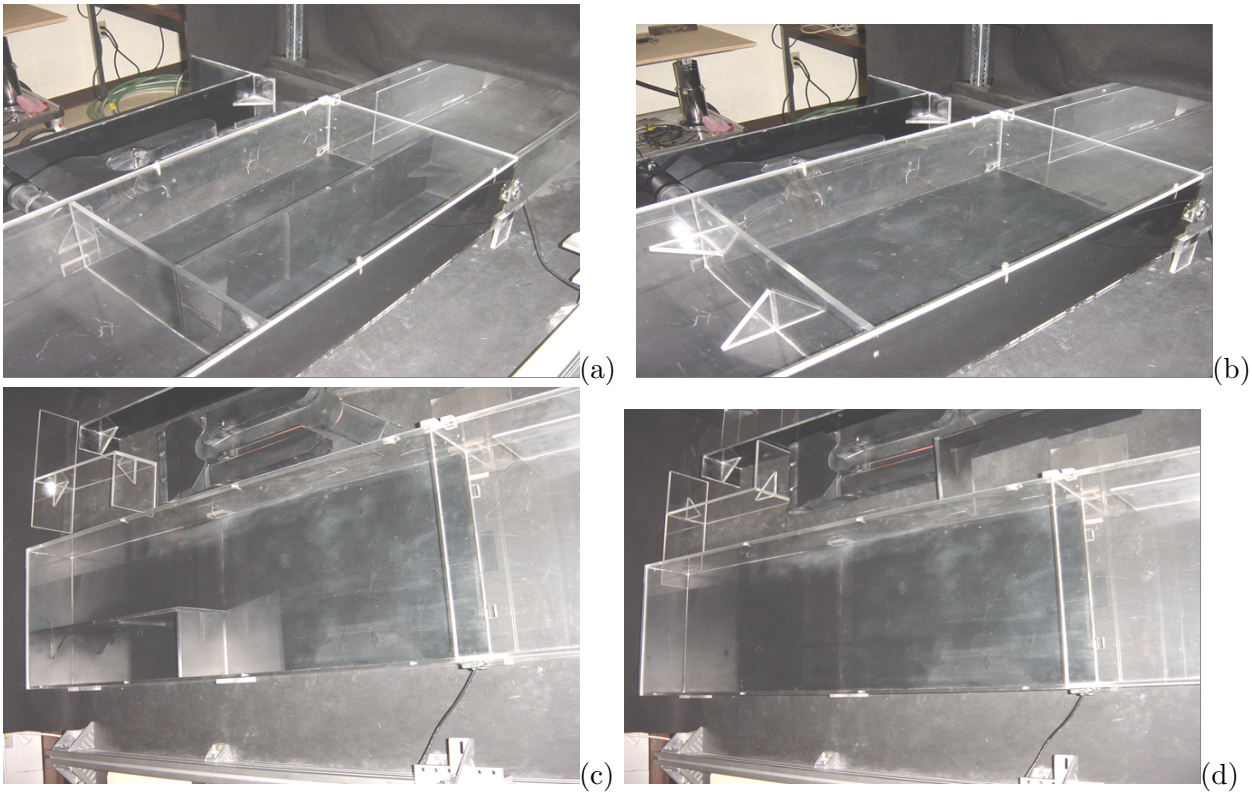

Figure 2.2: Pictures of the scaled physical models for 30 ft (a) and (b) and 60 ft (c) and (d) deep cuts with and without the slabs. These correspond to the sketches shown in Figure 1.2

2.2.2 Scrubber Model

The scrubber system for this modeling study did not exactly simulate an underground scrubber arrangement. Since the scrubber system could not be modeled exactly as it appears in a mine due to limited space and flow rate, a simplified model of the scrubber was simulated using an open ended 2 inch diameter PVC pipe. The airflow through this pipe was drawn by a suction system which is a part of the main dust collecting system in the building. The maximum airflow induced by the scrubber system corresponds to 0.93 m^3/s (200 cfm) (corresponding to 1.4 m^3/s (3,000 cfm) in a full-scale model) for the underground condition. For validation purposes two different arrangements with the scrubber were tested as shown in Figure 2.3. As shown in the Figure 2.3a, a cylindrical "scrubber" was simulated by straight PVC pipe placed in the middle on the entry floor, 1.5 m (5 ft) from the face for the "simplified scrubber model" and then as shown in Figure 2.3b the same PVC pipe was placed inside a continuous miner model, corresponding to the Joy Model 14CM Continuous Miner, located in the face area.

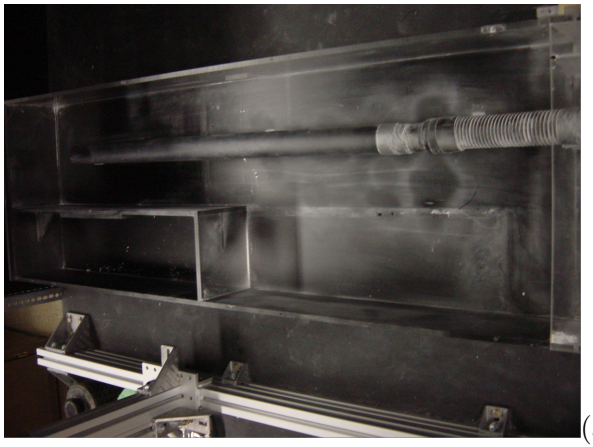
(a)

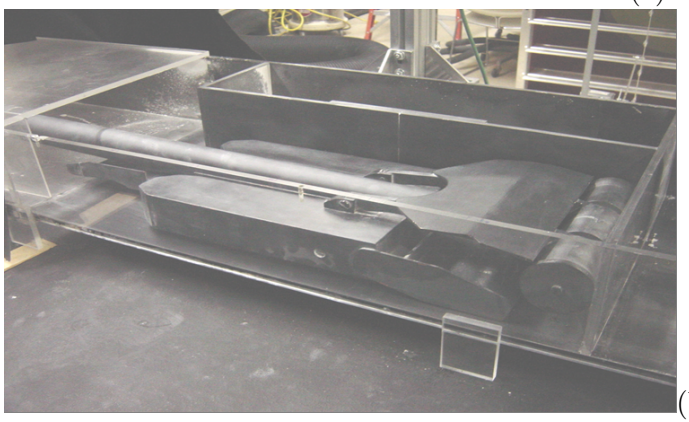
(b)

Figure 2.3: Two different arrangements with the scrubber system. (a) Simplified scrubber model. (b) Detailed machine mounted scrubber model.

2.3 Particle Image Velocimetry

Particle Image Velocimetry (PIV) is a technique where a planar laser light sheet is pulsed twice within a short time and images of particles in the light sheet are recorded on a high speed camera. The displacement of the particle images is measured in the plane of the image and used to determine the displacement of the particles in the flow. The most common way of measuring displacement is to divide the image plane into small interrogation windows and cross correlate the images from the two time exposures. To perform these measurements, tracer particles must be added to the flow field. The laser-light sheet illuminates these particles twice within a short, controlled time interval. The reflected (scattered) light is recorded either on a single frame or a sequence of frames by a CCD camera which is placed 90 degrees to the flow field. The displacement vector for each interrogation area is determined by means of a cross-correlation. It is assumed that all particles within one interrogation area have moved homogeneously between the two images. The projection

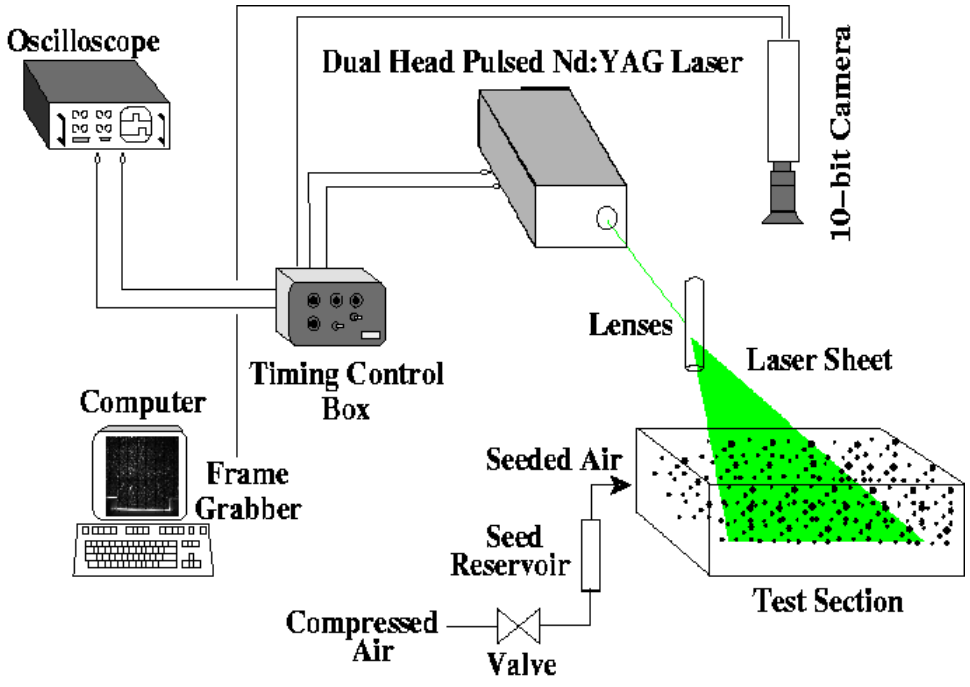

Figure 2.4: Schematic of the Integrated PIV system

of the flow vectors into the plane of the light sheet (two component velocity vector) is calculated taking into account the time delay between the two laser pulses and the image magnification factor. For more details see Adrian (1996), Grant (1994), and Raffel, et al., (1998).

The integrated PIV system being used in this study, seen in Figure 2.4 is comprised of the following components : laser and light sheet optics, image capture system, synchronizer, seed particle generator, image analysis and display and data analysis and post processing.

A New Wave, dual head, Nd:YAG Laser (532 nm wavelength with a 15 Hz repetition rate) is used to illuminate the particles. In a single head laser, there exists a time between the first laser pulse and second laser pulse. A CW laser is used if the flow is slow enough that streaking does not occur. But since the flow we studied is fast a double head laser was used where the time gap between the firing of first and second laser pulses is small and variable. The light sheet optics include both a cylindrical and spherical lens. The cylindrical lens diverges the laser beam into a sheet, and the spherical lens controls the light sheet thickness (about 1 mm at the focal length).

The particle images are recorded using a Roper Scientific-Kodak ES1.0, 10 bit, monochrome, dual channel digital camera, which contains a square, mega-pixel array 1018X1008. The ES1.0 is capable of taking a pair of images with a controllable delay time between the pair ranging from 1 microsecond to 1 millisecond.

The synchronizer controls the timing of the PIV system components (laser triggering, duration time between laser pulses, and camera triggering) and links the PIV system with a computer/frame grabber.

Talcum powder is used as seeding for most of the experiments. The reason for which baby powder was considered was due to their size (200 μm) which was considerably large enough to visualise and also quite suitable for such high flow fields where uniform distribution of seeding through out the flow is desired. The seeding was placed in a cylindrical vessel with a two hole lid, one for inlet of the Nitrogen gas and the other as the outlet for the seeding into the ventilating system. Nitrogen gas was used to stir the seeding and to have a free flow with uniform distribution in the air flow. For some runs SAFEX, oil based, smoke particle generator was used to make 1.0 μm size particles. The generator is adjustable, so that the density of the smoke could be controlled.

The CCD camera is used to grab sequence of images. Initially before capturing the image, the camera is adjusted for focus and clarity to see that it clearly defines each particle. Also a series of image pairs are initially captured to to see whether the seeding is more and less and is adjusted accordingly. Then series of images are captured using the XCAP frame grabber and array processing software.

After obtaining a series of images (typically 102 images or 51 pairs of images) using XCAP, a single image pair is examined in XCAP to see that the displacement between two sucessive particles is on a same scale for all image pairs. A 10-bit mask is then made which helps to mask of the unwanted region and later it is converted as a 8-bit mask in MATLAB. Input files and list files are created for each scenario with 32 X 32 or 64 X 64 window size (interrogation region) and a step size of 16 or 32. The WaLPT algorithm of Sholl and Savas (1997) is used for post processing these image pairs to get outputs of velocity vectors (u, v) and gradient tensor,

$$u_{ij} = \begin{pmatrix} \partial u/\partial x & \partial u/\partial y \\ \partial v/\partial x & \partial v/\partial y \end{pmatrix}$$

remove indent at each point, from which derived quantities such as vorticity can be calculated. The binary images are then succesively read into a MATLAB program which determines the average velocity field and other quantities such as RMS velocities, circulation and vorticity. The final result, which is a MATLAB file, is then converted to a *.dat file and then loaded in TECPLOT to get the velocity vector plots, streamline plots, pressure plots etc. The MATLAB codes and the sample input files are in Appendix A.

Chapter 3

Blowing Ventilation System Results

The parameter space that determines the number of possible scenarios for testing in such a validation study is large. Seven different scenarios representing the possible coal mining sequences with a blowing ventilation system have been considered and are shown in table 3.1. Here '**L**' is the depth of the cut, '$\boldsymbol{W_c}$' is the curtain width, '**H**' is the entry height, '$\boldsymbol{W_f}$' is the face zone width, '$\boldsymbol{V_{in}}$' is the inlet velocity, ' **EP**' is the scenario with the miner machine present in the face area and '**X**' is the physical parameter (control factor) being varied in that particular case. Each case is discussed in an individual section.

CASE	**L** (ft)	$\boldsymbol{W_c}$ (ft)	**H** (ft)	$\boldsymbol{W_f}$ (ft)	$\boldsymbol{V_{in}}$ (fpm)	**EP**	**X**	**A**	**B**	**C**	**D**
I	30	2	7	-	5000	No	$\boldsymbol{W_f}$	12	20	-	-
II	60	2	7	-	5000	No	$\boldsymbol{W_f}$	12	20	-	-
III	30	2	7	-	5000	Yes	$\boldsymbol{W_f}$	12	-	-	-
IV	30	2	7	12	-	No	$\boldsymbol{V_{in}}$	2900	3800	5700	-
V	30	2	-	12	5000	No	**H**	7	5.5	-	-
VI	30	2	7	-	5000	No	$\boldsymbol{W_f}$	12	14	16	20
VII	30	-	7	12	5000	No	$\boldsymbol{W_c}$	1	2	4	-

Table 3.1: Experimental cases examined.

3.1 CASE I

In all the cases presented below, the units correspond to full-scale equivalent. To obtain the actual dimensions used in the model, divide by 15.

3.1.1 *CASE IA*

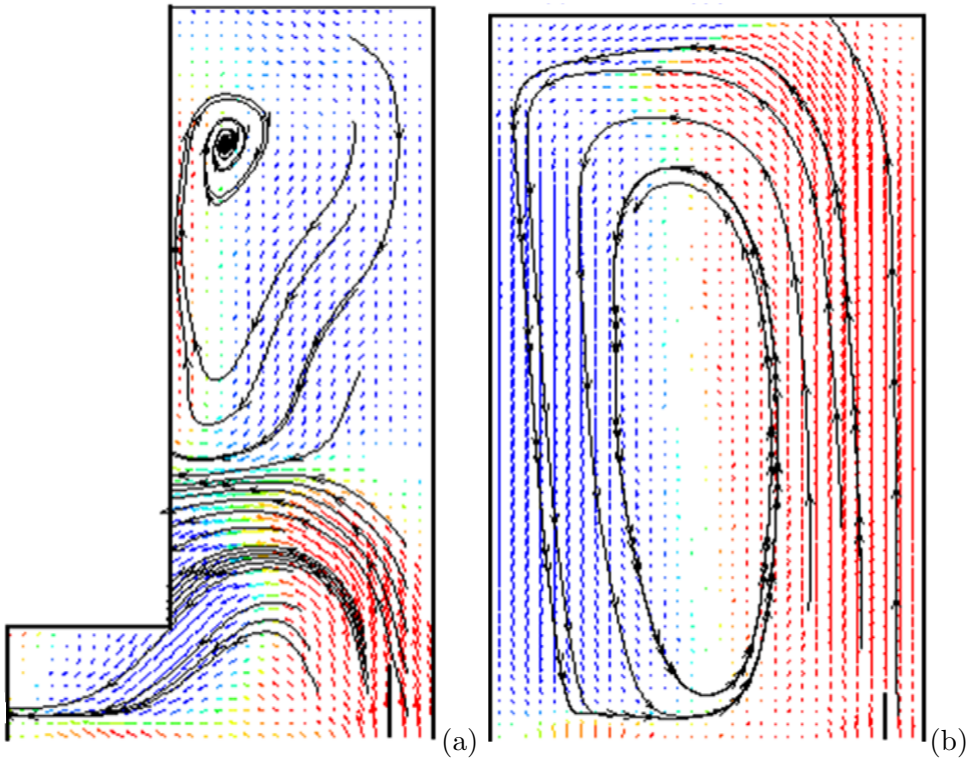

Figure 3.1: Sample velocity vectors from PIV measurements; CASE IA (a) and B (b), mid-plane.

The tested scenario is as follows: ventilation air of 2.5 m^3/s (5,300 cfm) is delivered to the 2.1 m (7 ft) high and 6.1 m (20 ft) wide entry with a 3.6 m (12 ft) wide and 9.1 m (30 ft) deep box cut by a blowing brattice with a setback of 10.3 m (35 ft). The two-dimensional velocity field (flow vectors) for a horizontal planes at half the height of the test section are determined by PIV as seen from Figure 3.1a, the primary ventilation air leaving the brattice mouth is a free jet that penetrates into the box cut for a distance of approximately 2.0 m (6 ft) and then separate from the wall (rib). It later reverses and creates a recirculation region in the face area. This reduces the air distribution in the face area and thus results in poor ventilation. This separation is very unstable and it is difficult to predict the exact location where the jet is separating.

Around 70% of the air turns into the main return while the rest of it continues to flow towards the face in the opposite direction, creating major recirculation region in the face region. This flow behavior was recognized and mentioned briefly by previous researchers (Taylor, et al. (1992), Thimons, et al. (1999) and Thimons, et al. (2001). The authors identified this flow behavior as the **"Figure 8"** flow pattern.

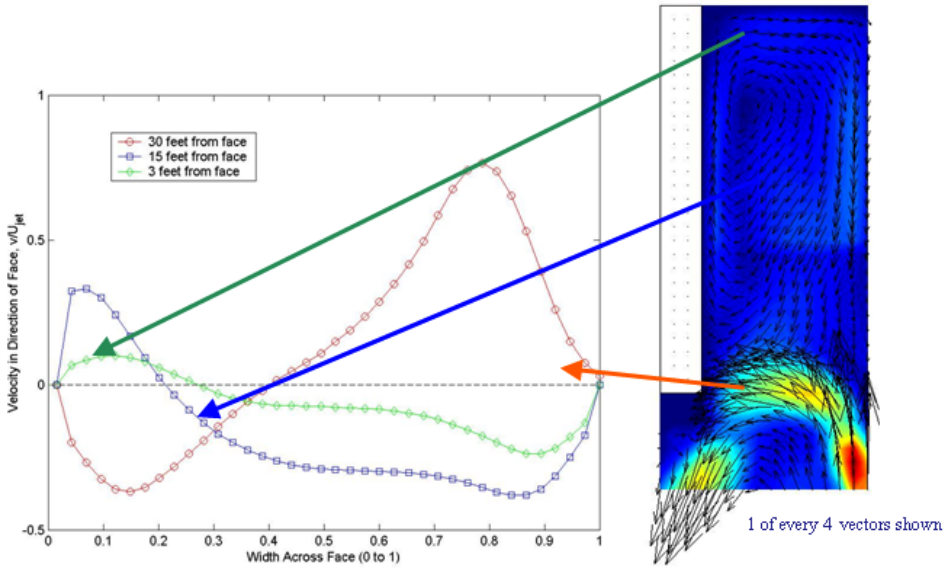

Figure 3.2: Velocity profiles for 35 ft deep cut with a slab.

To understand the flow more clearly, velocity profiles at three different locations in the flow for 30 ft deep cut with a slab were considered. The profiles were considered for distances 30 ft, 15 ft and 3 ft from the face. As we can see from Figure 3.2, the first profile for 30 ft down the face, the flow is positive and still penetrating towards the face. The next profile, for 15 ft from the face we observe a reverse flow. Similarly for 3 ft from the face, we see a reverse flow with very low velocity directed towards the face area.

3.1.2 *CASE IB*

In this scenario the slab cut is complete and the entry width is 6.1 m (20 ft), which is the whole length from the brattice mouth to the face. As can be seen from Figure 3.1b, the air penetrates into the face, sweeps the face with a strong air current and turns into the main return. We no longer observe the unsteady flow separation. This is a less hazardous situation which dilutes the methane gas considerably. As we increase the channel depth more than 9.1 m (35 ft), there tends to be separation occuring. This might be due to the build up of high pressures in the face area and is discussed below.

3.2 CASE II

3.2.1 *CASE IIA*

For the next two scenarios are similar to the scenarios described as CASE IA and B. The only difference between these two is the brattice setback that is now 18.3 m (60 ft). The measured two-dimensional flow distribution across the entire face area at the middle of the entry height is shown in Figure 3.3a. The characteristic flow separation is observed with a recirculation region in the face area. One thing can be observed from this velocity vector plot and from Figure 3.1, we see that the flow gets separated as soon as it encounters a wall. If we consider this flow as a jet emerging from an opening, the jet spreads and then it hits the wall towards the slab side and separates and reverse flow occurs in the face area. From Figure 3.1, the separation occurs at a distance of about 4 to 5 ft from the curtain, that is, the start of the slab. Similarly from Figure 3.3a, the flow got separates at a distance of 4 to 5 ft from the curtain.

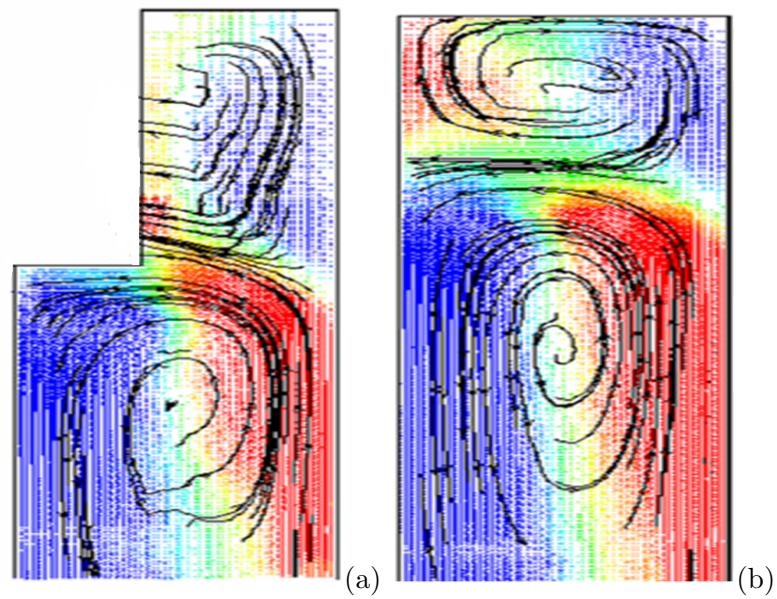

Figure 3.3: Sample velocity vectors from PIV measurements; CASE IIA (a) and B (b), mid-plane.

3.2.2 *CASE IIB*

With the slab completed and an entry width of 6.1 m (20 ft), the ventilation air, according to CASE IB, should penetrate into the face and turn into the main return. But as mentioned previously as we increase the depth of the channel, as can be seen from the data Figure 3.3a, the ventilation air reaches a certain distance close to the face and then separates from the wall. The

bulk of this flow turns into the return while the rest of it continues to flow towards the face in opposite direction creating a large recirculation region in the face area. So the 60 ft deep cuts have been the most problematic scenarios in this study. As mentioned in the previous section, the flow is separated as soon as it encountered a wall, but unlike such behavior the from the Figure 3.3b, the flow separates with no presence of the slab (or the wall). One reason might clearly explain both these phenomenon. As said, if the flow is considered as a jet emerging from an openings within confined walls, this jet spreads wider downstream. Perhaps for this case the jet was spreading resulted in a reverse flow in the face region. Another factor causing flow separation are the adverse pressures in the face, which shall be discussed later.

3.3 CASE III

3.3.1 *CASE IIIA*

This scenario is identical to CASE IB with the exception that the mining equipment is present at the face area. During these experimental studies, to simulate the mining equipment, a scaled model, as shown in Figure 3.4a corresponding to the Joy Model 14 CM (Continuous Miner) was placed in the face area. The flow distribution in the entire face area was measured for two different planes, one mid-plane of the miner as shown in Figure 3.4c and other above the miner machine Figure 3.4d. Figure 3.4b shows the raw data for the case where the laser is hitting at the mid-plane of the miner. For these two cases, the air behaves similar as for empty entry, penetrating to the face along the right wall for both levels.

3.4 CASE IV - Different inlet flow rates

Experimental results involving different flow rates are discussed in this section. Figure 3.5 compares the velocity vectors for three different inlet flow velocities of 2900 fpm (1127 cfm), 3700 fpm (1438 cfm) and 5700 fpm (2215 cfm), respectively.

3.4.1 *CASE IVA*

For the scenario discussed in section 3.1.1, the inlet velocity was kept low at 2900 fpm for this case. From Figure 3.5a, the lower velocity did not help and the flow separated immediately downstream of the curtain.

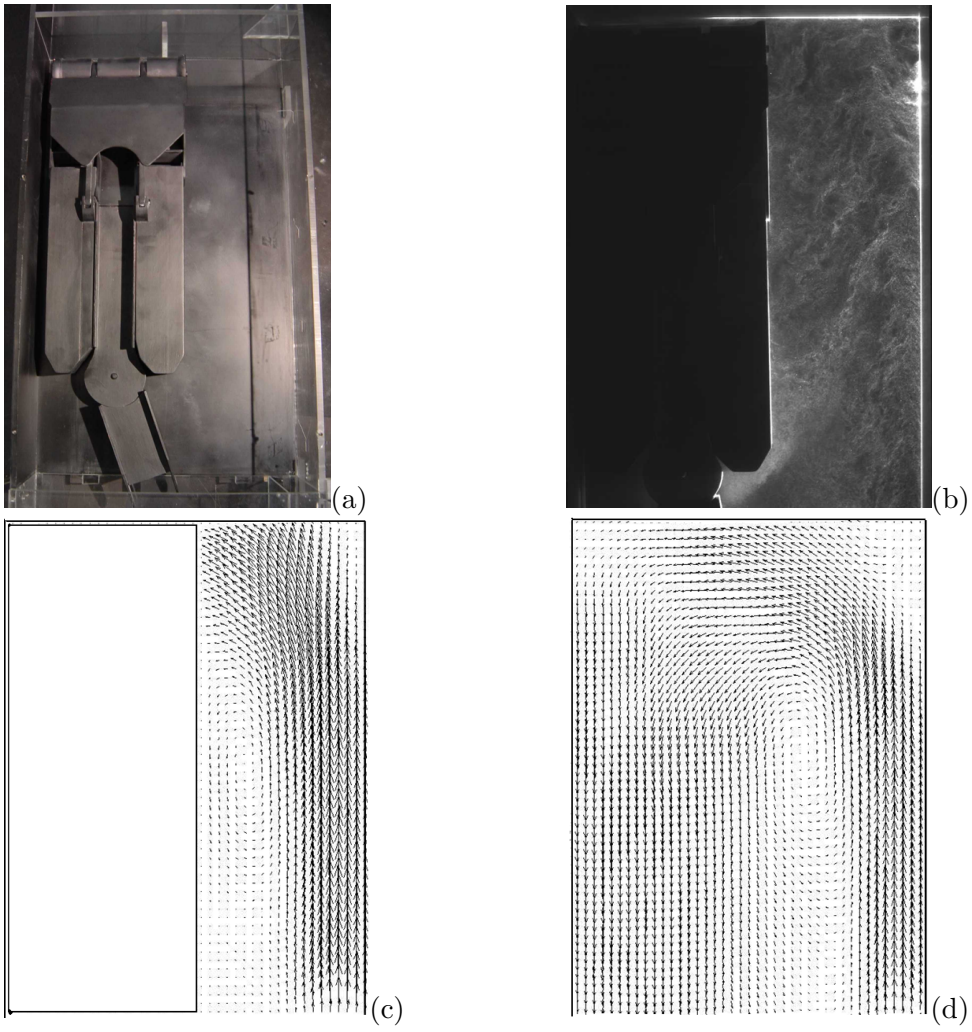

Figure 3.4: Picture of the scaled model of the miner machine (a) and rawdata with the miner machine position (b); Sample velocity vectors for CASE IIIA; laser hitting at the mid-plane of the miner (c) and above the miner (d).

3.4.2 *CASE IVB*

The inlet velocity for this case was increased to 3800 fpm. Figure 3.5b shows the velocity vectors for this case. The flow penetration is the same as discussed in the CASE IVA. The increase in inlet flow velocity did not aid in providing better air distribution in the face area.

3.4.3 *CASE IVC*

The inlet velocity for this case has been increased to 5700 fpm, the maximum attainable. From Figure 3.5c, the flow penetration is sightly less than the previous two cases and it remains constant.

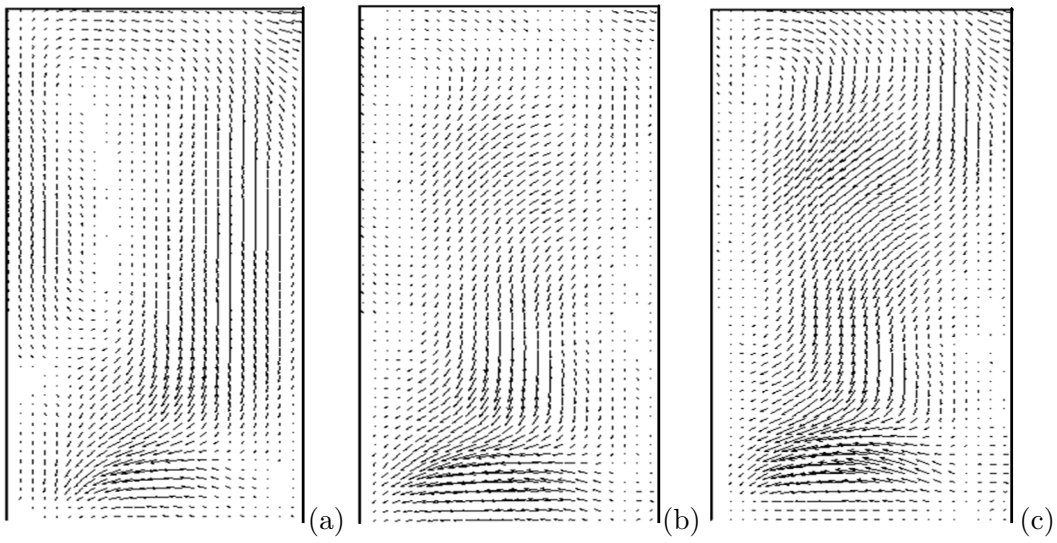

Figure 3.5: Comparison of velocity vectors for different flow rates for CASE IVA, CASE IVB and CASE IVC.

This velocity too did not provide good face ventilation.

Figure 3.5, though there has been an increase in the inlet flow velocites, the penetration of air is not much improve and after a certain value it remains constant. Varying the inlet flow rates did not really help to provide good air distribution in the face area. Thus higher flow rates do not necessarily mean better ventilation.

3.5 CASE V - Different entry heights

As a part of the parametric study, the second parameter considered was the variation of the entry height '**H**' of the model. Experiments for two different entry heights of 2.14 m (7 ft) and 1.68m (5.5 ft) were performed and are discussed as CASE VA and B. For each of the cases, the height was uniform across the model observation region.

3.5.1 *CASE VA*

This scenario was discussed in section 3.1.1 with the slab in position. From the discussion in section 3.1.1, it can be seen that the flow was separated with a poor air distribution in the face area.

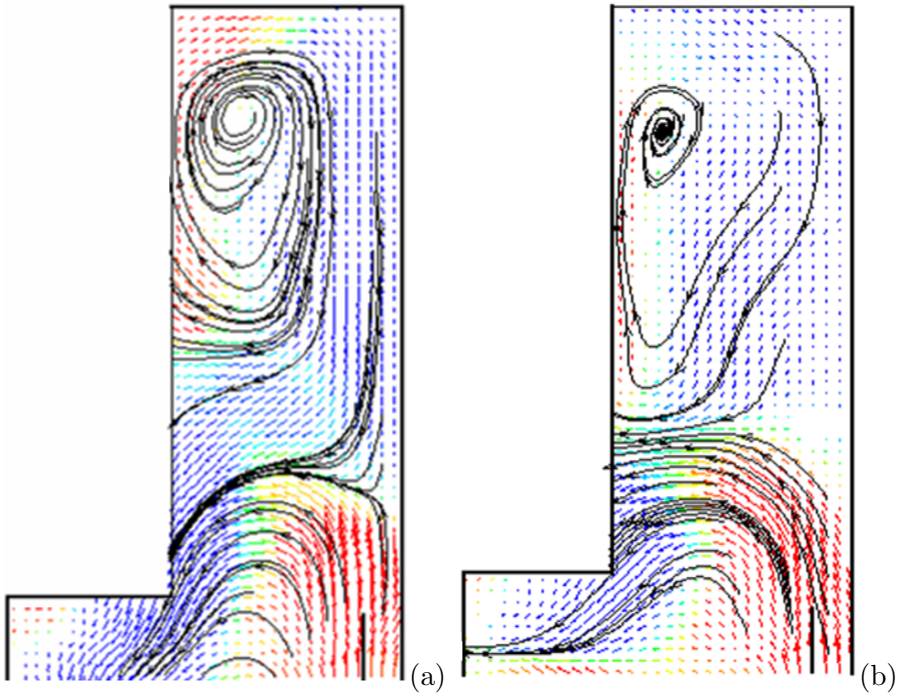

Figure 3.6: Comparison of velocity vectors for different entry heights for CASE VA and CASE VB.

3.5.2 *CASE VB*

Another value for the entry height of 1.68 m (5.5 ft) was considered for the study. But from the Figure 3.6b, for this case too the flow though penetrated a little more deeper than the CASE VA but still was separated with a recirculation region in the face area. Thus this scenario was not of much help in improving the air distribution in the face area. The effect of this parameter on the flow distribution is negligible.

3.6 CASE VI - Different face zone widths

The third parameter considered for the parametric study was the variation of the face zone widths and the present section discusses these results. It was observed from the experimental data, that the flow separation phenomena was mostly affected by the width of the face zone to which the air is delivered. It is obvious that for all tested box cut scenarios with an entry width around 3.6 m (12 ft), the flow separates from the wall, but for slab cuts of 6.1 m (20 ft) and a fully developed entry, the ventilation air penetrates into the face. To be able to learn how this width effects the flow behavior, additional series of tests for entries of 4.3 m (14 ft) and 4.9 m (16 ft) wide were conducted. The curtain delivered an air quantity of 2.5 m^3/s (5,300 cfm). It should be noted that

these tests do not exactly simulate mining configurations as they are not practically available in actual coal mines.

3.6.1 *CASE VIA*

The tested scenario is as follows: ventilation air of 2.5 m^3/s (5,300 cfm) is delivered to the 2.1 m (7 ft) high and 6.1 m (20 ft) wide entry with 3.6 m (12 ft) wide and 9.1 m (30 ft) deep box cut by a blowing brattice with a setback of 10.3 m (35 ft) as shown in Figure 3.1a. As discussed in section 3.1.1, it can be seen that the air is separated far down from the face. 70% of the air returns to the main entry and the remaining flows into the face area in the reverse direction creating a large recirculation region. This case has poor air distribution and ventilation in the face area.

3.6.2 *CASE VIB*

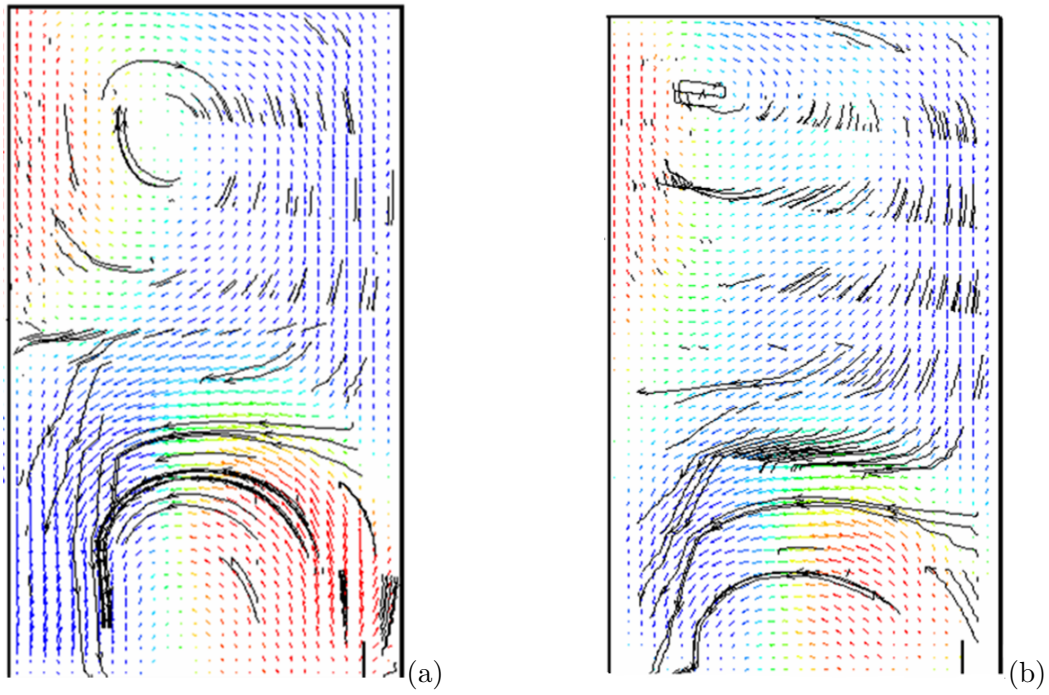

Figure 3.7: $\boldsymbol{W_f}$ = 14 ft, CASE VIB, Q = 1.6 m^3/s (3,500 cfm) (a) and Q = 2.5 m^3/s (5,300 cfm) (b), respectively.

Figures (3.7)a and b show the air flow patterns found in the horizontal, middle plane of the face area for the 1.6 m^3/s (3,500 cfm) and 2.5 m^3/s (5,300 cfm) scenarios, respectively for $\boldsymbol{W_f}$ = 4.3 m (14 ft). So as can been from these behaviors the flow is separated similar to the case of 3.6 m (12 ft) from the wall and recirculates in the face area.

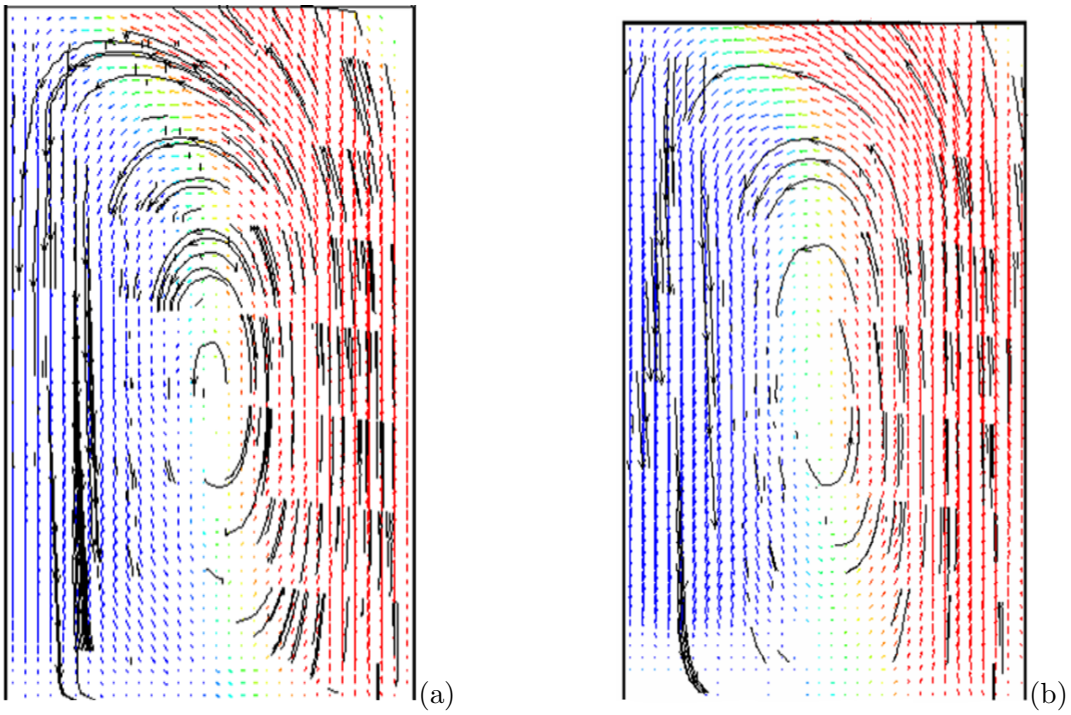

Figure 3.8: $\boldsymbol{W_f}$ = 16 ft, CASE VIC, Q = 1.6 m^3/s (3,500 cfm) (a) and Q = 2.5 m^3/s (5,300 cfm) (b), respectively.

3.6.3 *CASE VIC*

Figures (3.8)a and b shows the air flow patterns found in the horizontal, middle plane of the face area for the 1.6 m^3/s (3,500 cfm) and 2.5 m^3/s (5,300 cfm) scenarios, respectively for $\boldsymbol{W_f}$ = 4.9 m (16 ft). Comparing the flow fields for 3.6 m (12 ft) and 4.9 m (16 ft), it can be seen that as the entry width is increased the flow of air towards the face penetrates deeper. From the face zone width of 4.9 m (16 ft), the jet flow became narrowed and distribution of air in the face area improved.

3.6.4 *CASE VID*

This scenario discussed in detail in section 3.1.2 has the slab cut complete and the entry width is 6.1 m (20 ft), from the whole length from the brattice mouth to the face. The flow no longer separates from the wall. The jet is narrower than the previous CASE IVC and has good air distribution in the face area.

From Figure (3.9), it can be seen that as the entry width was increased from 12 ft to 20 ft, the penetration of air towards the face has been deeper and for the entry width of 16 ft the flow was

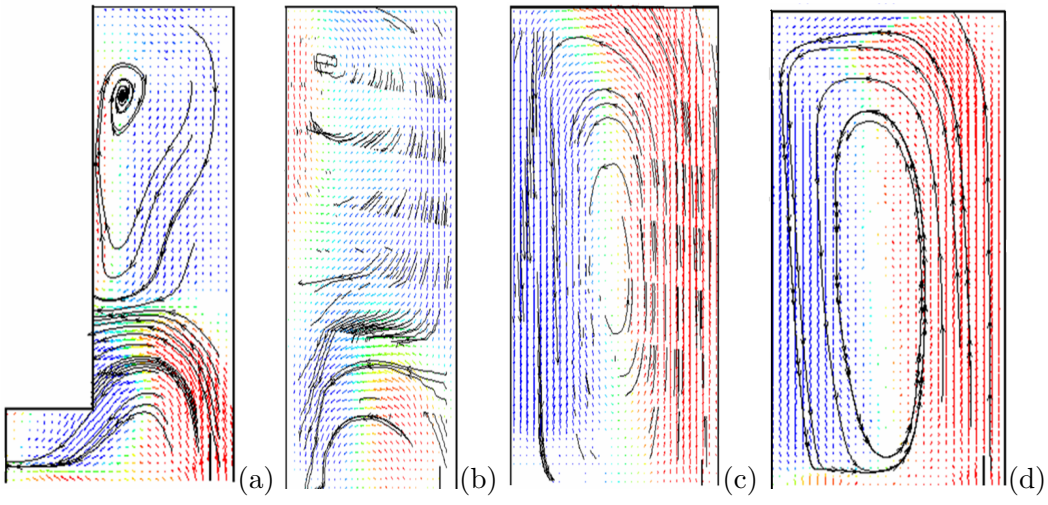

Figure 3.9: Comparison of velocity vectors for different face zone widths for CASE VIA, CASE VIB, CASE VIC and CASE VID.

carried to the face area. This flow is basically a jet flow emerging from an opening into a confined region. For the CASE IA of 12 ft entry width, the jet with a large spreading angle got separated with a large recirculation region in the face area. Now when the width is increased to 16 ft, the jet became narrower and then it hit the face wall and made a U-turn, thus sweeping the face area. Similar is the case with a 20 ft wide entry width. More detailed study about this jet behavior has to be performed in the future.

3.7 CASE VII - Different curtain widths

Last parameter of the parametric study done and verified was the effect of various curtain widths and this section shows the results concerning that arrangement. These curtain widths considered were typical mining configurations. Three different curtain widths of 0.306 m (1ft), 0.6125 m (2 ft) and 1.225 m (4 ft) were considered. Figures 3.10a, b, and c compare the stream line plots for these three different curtain widths of 0.306 m (1 ft), 0.6125 m (2 ft) and 1.225 m (4 ft) respectively.

3.7.1 *CASE VIIA*

The curtain width was reduced to 0.306 m (1ft) for this particular case. The decrease in the curtain width increased the dynamic velocity of the jet emerging from the curtain and helped penetration in the face area. This case is feasible in the real mining situations and might be worthy

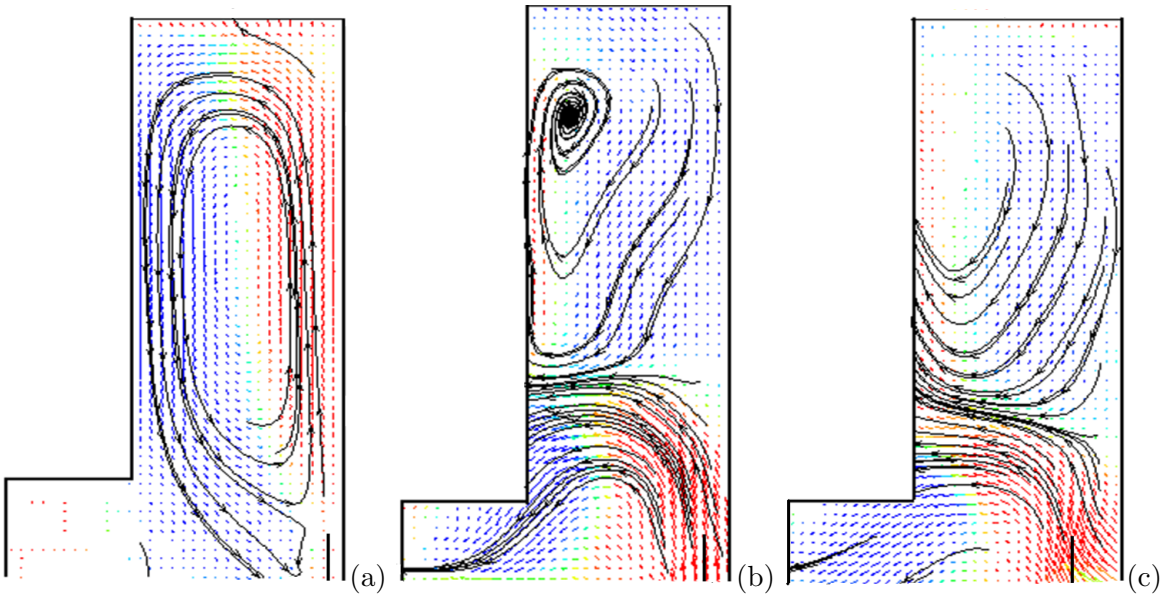

Figure 3.10: Comparison of velocity vectors for different curtain widths for CASE VIIA, CASE VIIB and CASE VIIC.

of consideration by the mining industry.

3.7.2 *CASE VIIB*

This scenario is the same as discussed in section 3.1.1. The flow separation further down from the face and the large recirculation region has reduced the chances of having good air distribution and ventilation in the face area.

3.7.3 *CASE VIIC*

The curtain width for this case has been increased to 1.225 m (4 ft). The increase in the curtain width has reduced the dynamic velocity thus spreading the jet wider than the previous two cases. This scenario does not result in good air distribution and face ventilation.

The decrease in curtain widths increases the dynamic velocity of the flow making the jet more and more narrower. From Figure 3.10a, for 4 ft curtain width, there was a very wide jet emerging from the curtain and it lacked the required dynamic energy for it to penetrate deeper. But from Figure 3.10b, as the curtain width was reduced down to 2 ft, the penetration of jet was a little deeper than 4 ft curtain width, due to increase in the jet momentum. From Figure 3.10c, for a curain width of 1 ft, the jet is much narrower than the other two cases, and has sufficient dynamic energy to overcome the reversal caused by adverse pressure gradient in the face area.

3.8 Characteristics of the Wall Bounded Spreading Jet

3.8.1 *Introduction*

The wall bounded jet had only one degree of freedom. Its vertical spread was confined due to the closed system and was limited by the entry height of 2.14 m (7 ft). Some of the variables characterizing the wall jet are calculated and presented in the present section. The diffusion of the jet was characterized by the velocity decay coefficient value and the lateral spread of the jet was determined by the spreading angle β. The value of the virtual origin x_p was also determined. The virtual origin is the point on the **X** axis from which the jet appears to originate, when the line connecting the half-widths is extended back to the axis. This particular study of wall jet characteristics were recognized and mentioned briefly by previous researchers (Kirkpatrick et al., 1998). The values for the spread angles β and virtual origins x_p were determined from the MATLAB code and the values of the velocity decay coefficients was calculated using the following equation where K is the velocity decay coefficient, u_m is the maximum velocity, u_o is the effective outlet velocity, A_o is the effective outlet area, x is the depth of the model considered and x_p is the virtual origin.

$$\frac{u_m}{u_o} = K\frac{\sqrt{A_o}}{x + x_p}$$

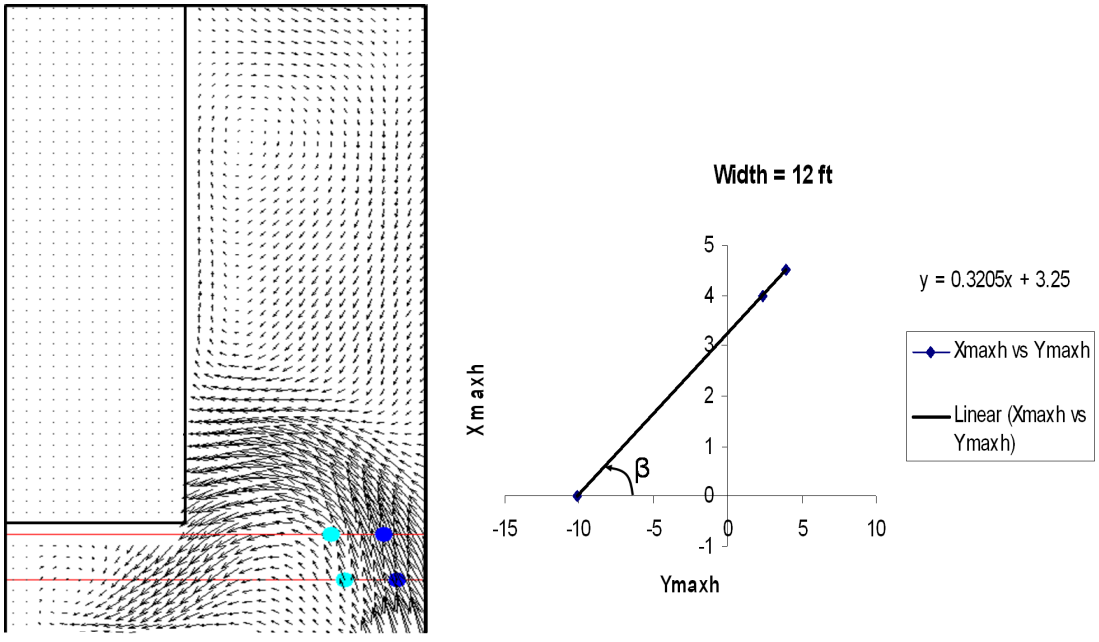

Figure 3.11: Calculation of β and x_p values for 30 ft deep cut with a face zone width of 12 ft.

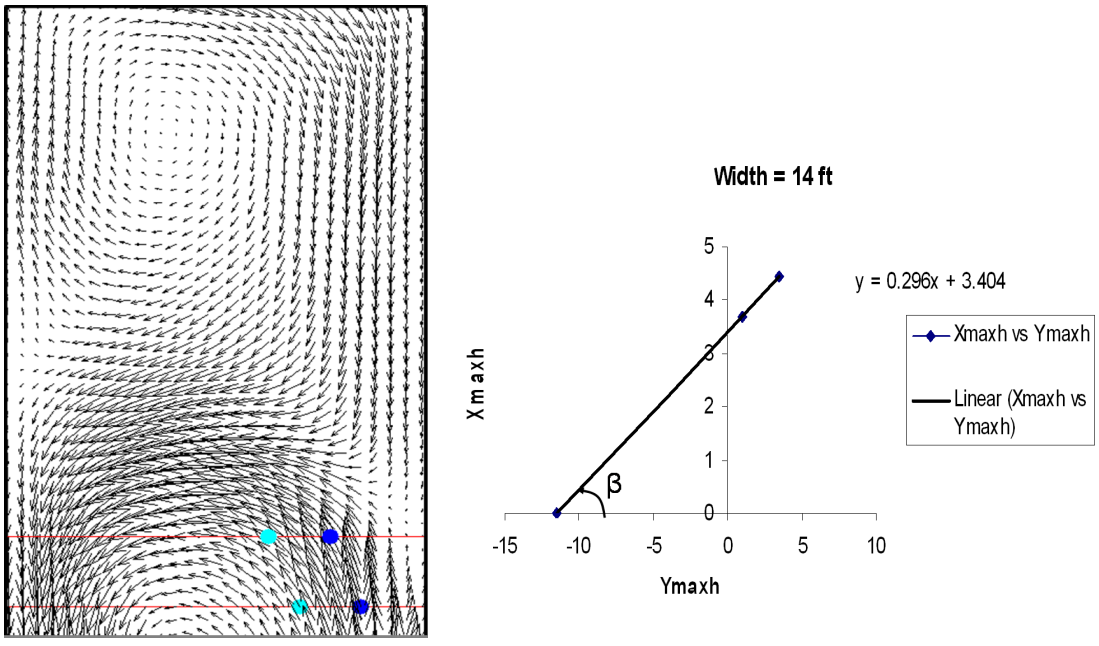

Figure 3.12: Calculation of β and x_p values for 30 ft deep cut with a face zone width of 14 ft.

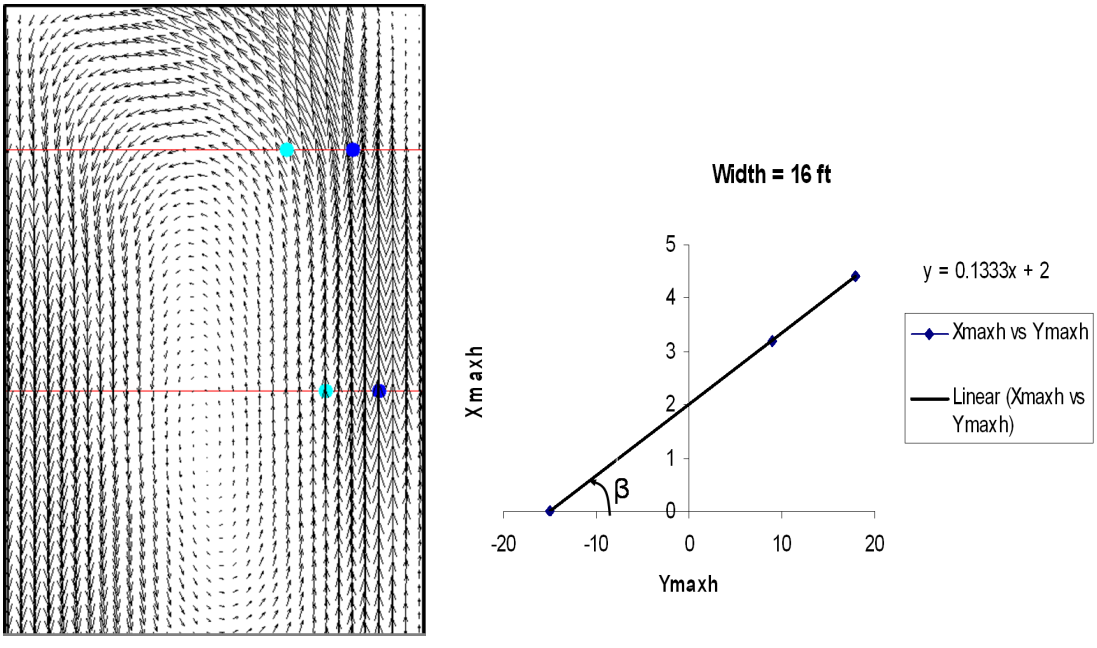

Figure 3.13: Calculation of β and x_p values for 30 ft deep cut with a facezone width of 16 ft.

3.8.2 *Calculations of β and x_p values for different face zone widths*

The calculations for the β and x_p were done considering the half values of the maximum velocities $V_{max1/2}$ as discussed in the journal paper by Kirkpatrick et al., (1998). All of these

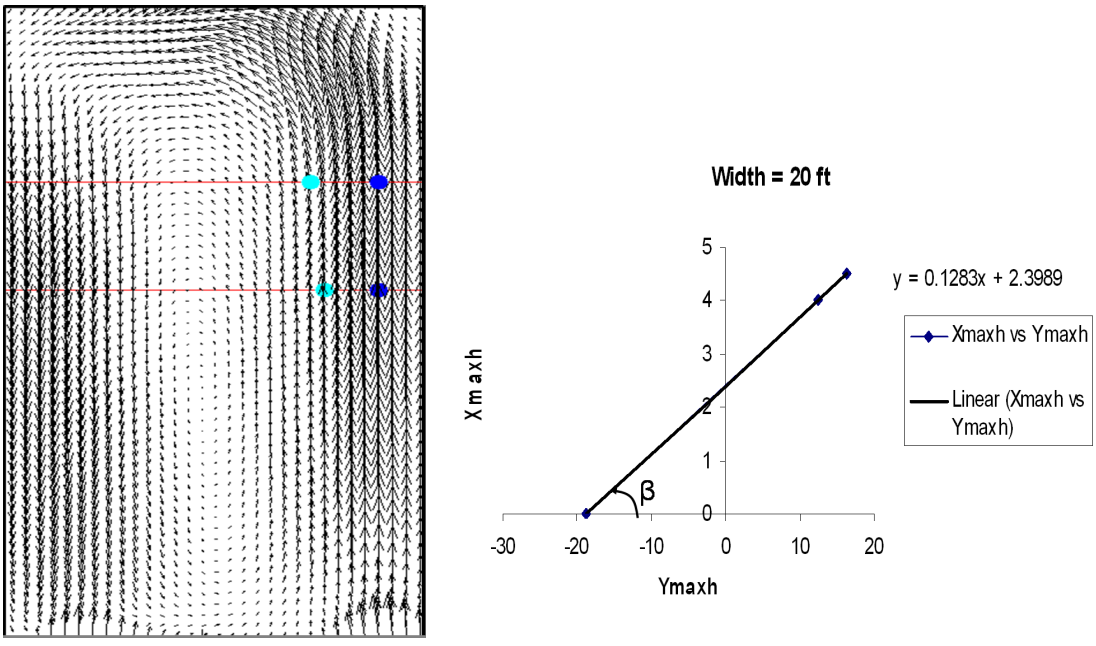

Figure 3.14: Calculation of β and x_p values for 30 ft deep cut with a face zone width of 20 ft.

calculations were done for the scaled physcial model. The location of these $V_{max1/2}$, that is, xmaxh and ymaxh were obtained directly from the MATLAB code. From Figure 3.11, for each particular row, the MATLAB locates the position of the $V_{max1/2}$ (represented by the cyon color dots). Then these values of xmaxh and ymaxh were plotted in a spread sheet and the slope of the line joining these points gave the value of β. On extending this line further back to the negative X-axis, the values of x_p can be calculated. The same procedure was repeated considering different widths at the face zone as shown in Figures 3.11, 3.12, 3.13 and 3.14. From Figure 3.11 for a face zone width of 12 ft, two rows with the x-coordinates ranging from 10.0 to 11.25 cm and y-coordinates ranging from 5.85 to 9.75 cm on the scaled model were considered for the location of the $V_{max1/2}$. Then as mentioned above these x and y coordinates were plotted and the values of β and x_p were calculated. For a face zone width of 14 ft from Figure 3.12, two rows were considered with x and y coordinates for the location of the $V_{max1/2}$ ranging from 9.25 to 11.1 cm and 2.5 to 8.75 cm, respectively. Now plotting these coordinates gave the values of β and x_p. For a face zone width of 16 ft, from 3.13, two rows with x and y coordinates for the location of the $V_{max1/2}$ ranging from 8 to 11 cm and 22.5 to 45 cm were considered, respectively. These x and y coordinates were plotted to determine the values of β and x_p. For the face zone width of 20 ft, the x and y coordinates for the location of the $V_{max1/2}$ ranged from 10.0 to 11.25 cm and 31.2 to 41.25 cm, respectively. These were plotted in the similar behavior as discussed above to obtain the values of β and x_p. For the different face

zone widths of 12 ft to 20 ft, the β values ranged from 35° to 8.132° and the x_p values ranged from 7.43 in to 31.5 cm on the physcial model.

3.8.3 *Calculations of β and x_p values for different curtain widths*

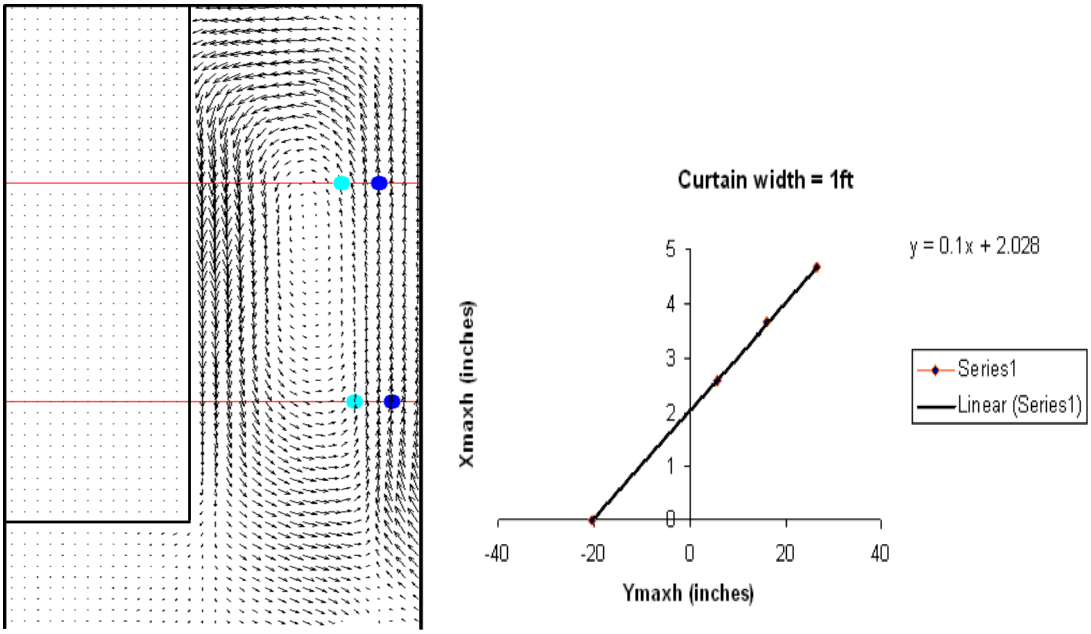

Figure 3.15: Calculation of β and x_p values for 30 ft deep cut with a curtain width of 1 ft.

The calculations for β and x_p followed the same procedure as discussed in the section 3.8.2. Three different curtain widths of 1 ft, 2 ft and 4 ft were considered. For a curtain width of 1 ft, from Figure 3.15, two rows with x and y coordinates for the location of the $V_{max1/2}$ ranging from 7.5 to 8.75 cm and 21.5 to 41 cm were considered respectively. Similarly for the curtain width of 4 ft, from Figure 3.16, two rows with x and y coordinates for the location of the $V_{max1/2}$ ranging from 10 to 11.25 cm and 3.9 to 6.83 cm were considered respectively. The β and x_p values were then obtained from the spread sheet plots. The β and x_p values varied from 18.4° to 5.7° and 19.5 to 95.5 cm on the scaled model, respectively.

3.8.4 *Results and Discussion*

This particular study was conducted for two different scenarios of a box cut with 9.1 m (30 ft) depth. Variations of the $\boldsymbol{W_f}$ and $\boldsymbol{W_c}$ were considered. Table 3.2 below discusses the characteristics of the wall bounded jets under various parametric conditions.

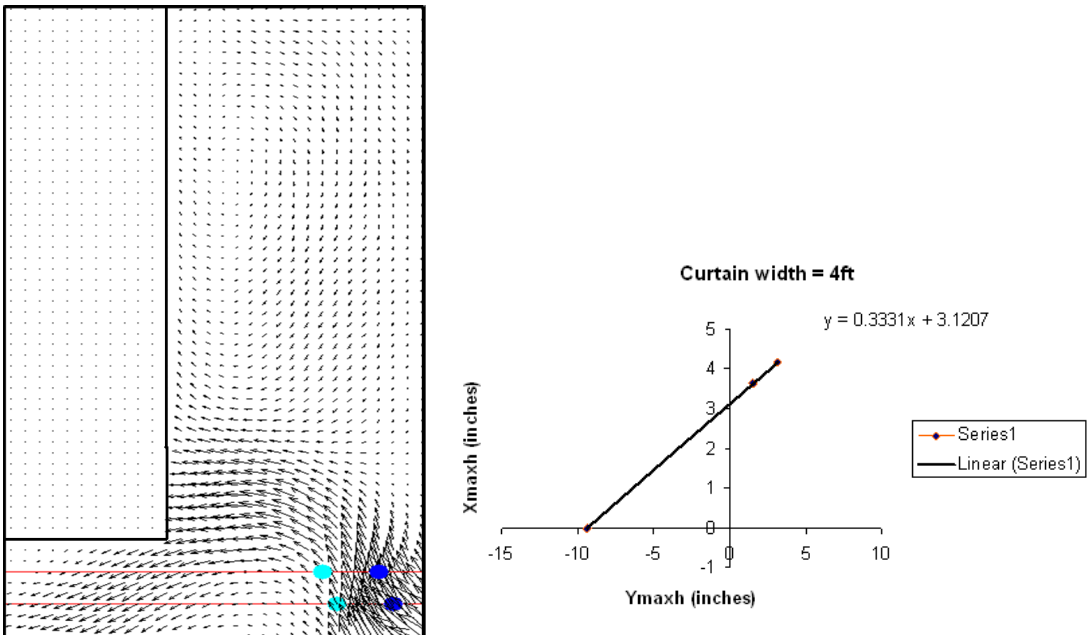

Figure 3.16: Calculation of β and x_p values for 30 ft deep cut with a curtain width of 4 ft.

Scenario	β	x_p	**K**
CASE IA	35	2.97	0.000161
CASE VIB	24.22	9	0.000234
CASE VIC	9.98	8.5	0.00590
CASE IB	8.132	12.6	0.000404
CASE VIIC	18.4	9.37	0.000107
CASE VIIA	5.7	20.28	0.000171

Table 3.2: Spread Angles, Velocity Decay Coefficients and Virtual Origins.

From the table we can see that, the spreading angles are largely effected by the entry widths and the curtain widths. As the entry widths are increased from 3.6 m (12 ft) to 6.1 m (20 ft), the spread of the jet has become more narrow. The β value for 3.6 m (12 ft) was about 35° and for 6.1 m (20 ft) it was 8.13°. We observed from the previous sections that 4.9 m (16 ft) was considered a critical entry width. At this particular entry width, the flow did not separate and penetrated all along to the face. So from our spread angle values it is observed that this entry width of 4.9 m (16 ft) is critical. The relation between the entry width and the spread angle β values were plotted and from the Figure 3.18 a prediction for the separation was clearly observed. For the entry width of 4.9 m (16 ft), the flow behaves very unstably with a "flip-flop" motion. It is the critical width where the flow actually tries to penetrate deep down into the face. The effect of the curtain widths

has beenvery prominent. As the curtain width was decreased from 1.225 m (4 ft) to 0.6125 m (1 ft), the spreading angles narrowed down from 18.4° to 5.7°. This clearly shows that narrowing down the curtain width from 1.225 m (4 ft) to 0.6125 m (1 ft) increases the dynamic velocity of the jet thus making it less wide and helping in penetrating greater depths. The velocity decay coefficient values were not exactly correlated with the theoretical values but they were similar to them.

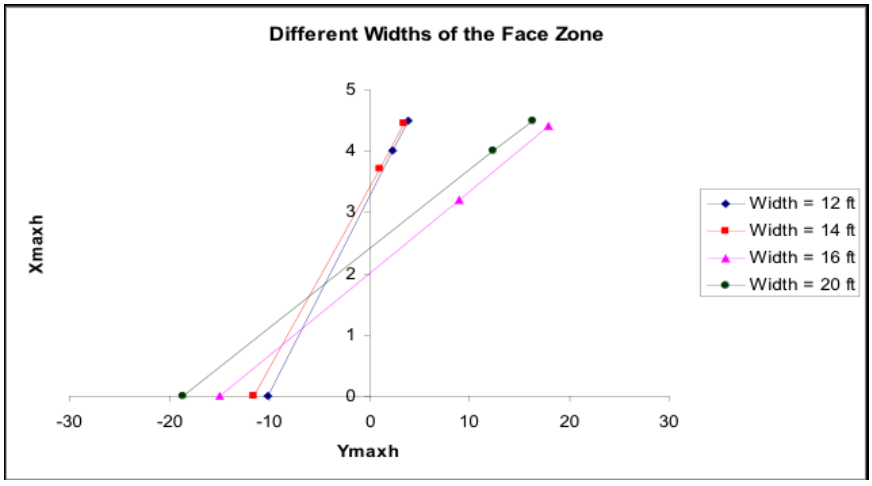

Figure 3.17: Comparison of β and x_p values for various face zone widths.

One of the parameters which helped to provide a good air distribution in the face area was the effect of variation of the face zone widths. The values of β from table 3.2 and various face zone widths were plotted in Figure 3.17. From observing the plot, it can be seen that as the width of the face zone became wider, the spreading angles β have become more and more narrower thus avoiding the flow separation.

3.8.5 Pressure Measurements for 30 ft deep cut

Static pressure measurements were conducted on the scaled model for the box cutting sequences with curtain setback of 9.1 m (35 ft) for CASE IA and CASE IB in Chapter 3. The pressure taps were punched at various locations along the model and using static taps static pressures were determined. It was observed a -525 kPa pressure was necessary for the air to penetrate all the way to the face. Filled pressure contours from the experiments and Fluent are shown in Figures 3.19 and 3.20. From the Figures 3.19a and 3.19b it can be seen that though experimental and the CFD data may not exactly correlate but had similar behavior. Also from the Figure 3.20, the jet spread is much wider for the experimental plot than CFD. The plots obtained by experiments do not clearly depict the flow behavior in the face region as does the PIV data.

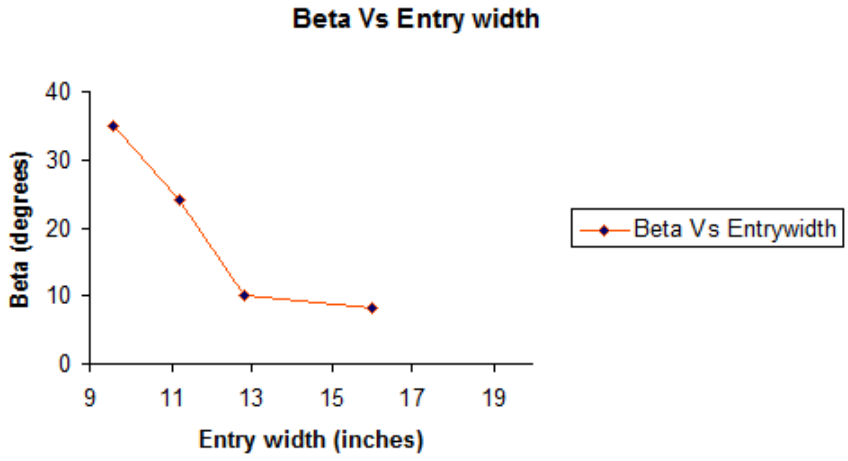

Figure 3.18: Relation between the β and face zone widths.

3.9 Summary

From the results presented in the above sections, it can be seen that the box cutting scenarios had problems with good air distribution at the face area. The mining scenario for 18.3 m (60 ft) setback brattice had problems with ventilation for both the slab and box cut too. The presence of the miner machine in the face area was a major flow obtruction and showed worst ventilation. To clearly understand what parameters are affecting the flow behavior a parametric study was conducted. The effect of varying inlet flow velocities, entry heights, entry widths and curtain widths were studied. From these studies, it was understood that the variation in inlet flow velocities and entry heights did not aid in bringing more air to the face area, whereas, the variation of entry widths and curtain widths were really helpful in providing more air into the face. A width of 16 ft was determined as the critical width. Calculations pertaining to understand this jet flow, too proved that these two parameters have considerable affect on the air flow.

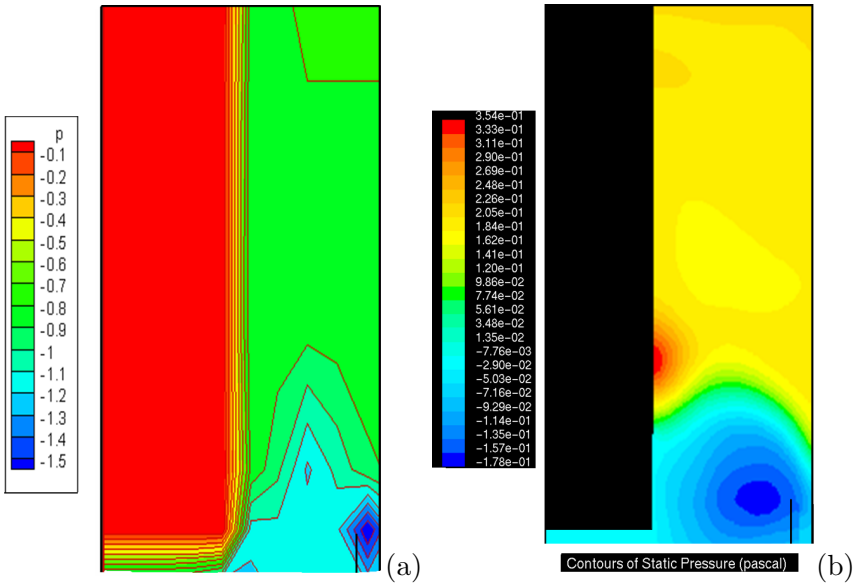

Figure 3.19: Pressure plots for CASE IA, experimental data plot (a) and CFD plot (b).

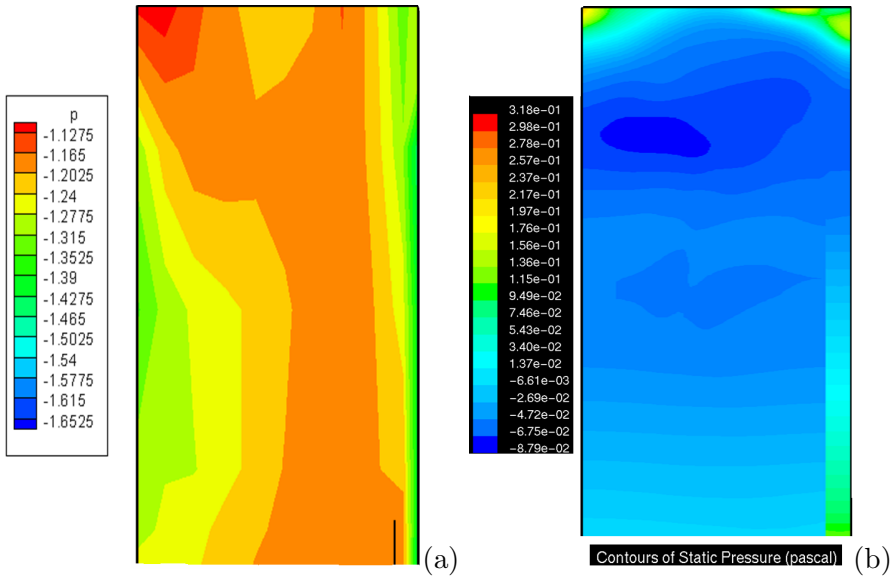

Figure 3.20: Pressure plot for CASE IB, experimental data plot (a) and CFD (b).

Chapter 4

Blowing Ventilation and Scrubber System Combined Results

4.1 Introduction

The effects of using a machine-mounted scrubber system in collecting coal dust and methane removal were first tested by Ingersoll-Rand using a 1:4 scaled physical model (Clouse,1982). These scrubber systems are essentially used to improve the coal dust collection in the face area so that the miner can have improved visibility during coal extraction. From these experimental studies, it was observed that these scrubbers are air-moving devices (ventilating device). To clearly understand the flow behavior and validate such a system, experiments were performed on the 1:15 scaled physical model using various scrubber models. Due to space limitations, the construction of an exact replica of a scrubber system was not possible, but a similar mechanism was used for the experiments. Studies were performed with the scrubber system for the two box cut scenarios with curtain setbacks of 35 ft and 60 ft. A exhaust pipe was used to model this system with a maximum airflow of about 1.4 m^3/s (3,000 cfm) for the underground conditions. The description of the experimental arrangement with the scrubber system is discussed in Chapter 2 in §2.2.2.

4.2 Box cut with curtain setback of 35 ft

Two different arrangements with the scrubber system in position were tested. First, as shown in Figure 4.1a the scrubber system was placed on the floor and secondly, as shown in Figure 4.1b the same scrubber system was placed on the top of the continuous miner model located in the face area. The scrubber was placed at a distance of 1.5 m (5 ft) from the face as shown in the Figure

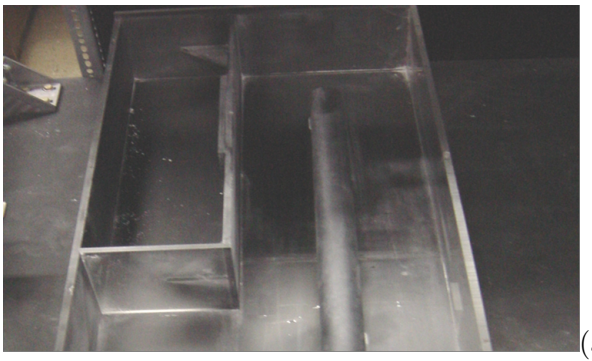
(a)
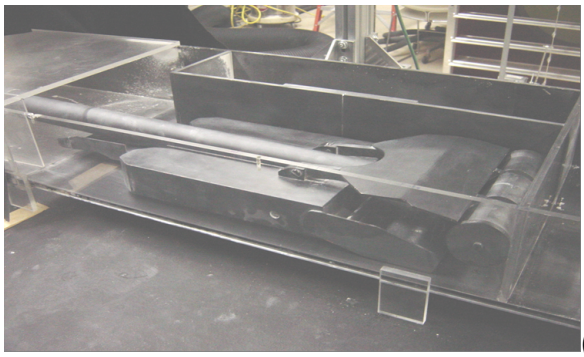
(b)
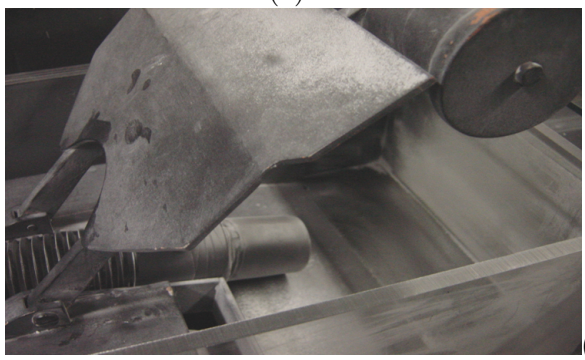
(c)

Figure 4.1: Scaled model for the simplified scrubber system (a) and for the machine mounted scrubber (b,c) for 30 ft deep box cut.

4.1c. PIV experiments were performed for both of these scenarios. From Figure 4.2 the streamlines for the case with and without the scrubber system can be compared. These results are with the simplified scrubber arrangement. From the figures, it can be seen that with the scrubber system in position, the air distribution in the immediate face area has improved. This encouraging result makes the 18.8 m (60 ft) deep cut mining possible.

Based on Ingersoll Rand studies, MSHA recommeded a ventilation ratio between the scrubber flow $\boldsymbol{Q_s}$ and the intake flow $\boldsymbol{Q_{in}}$ of close to one. But later studies performed by Taylor at el., (1996) and by Thimmons at el., (1999), showed there exists a complex relation between the ventilation ratios and the face ventilation performance. In order to learn more about the complexity of this relation, experiments were conducted for different ventilation ratios ranging from 14% to 53% on the 1:15 scaled physcial model. A one to one ratio could not be attained on the physical model due to system limitations. The minimum and maximum attainable ratio were 0.14 and 0.53, respectively. Tests were conducted for three different ventilation ratios of 0.14, 0.35 and 0.53. Figure 4.3 shows the streamline plots for three different ventilation ratios $\boldsymbol{Q_s}$ / $\boldsymbol{Q_{in}}$ of 0.14, 0.35 and 0.53. As can be seen from the plots, the penetration of air towards the face is more deeper with increasing ventilation ratio. The air distribution in the face area was much improved for the ventilation ratio

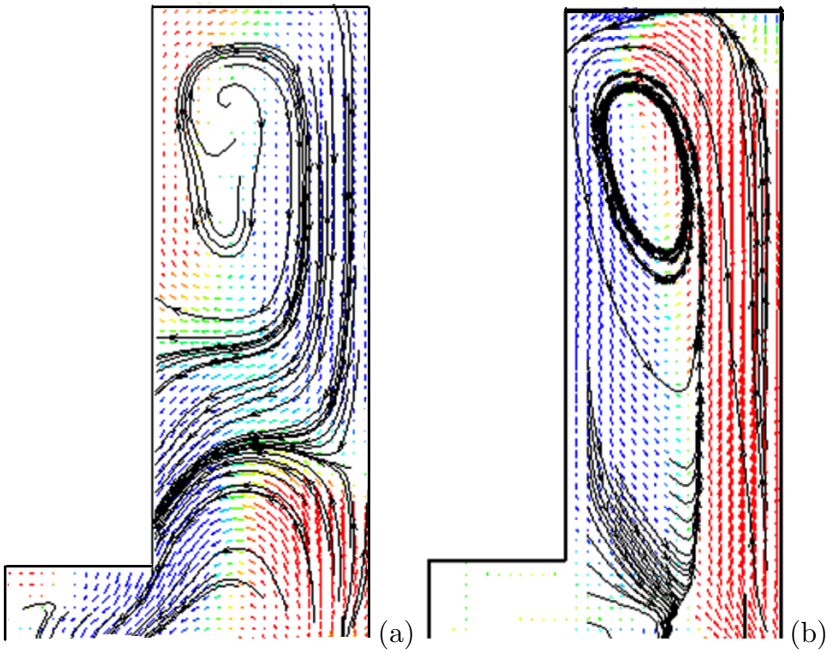

Figure 4.2: Streamlines from the PIV measurements with no scrubber (a) and (b) for simplified scrubber model for a 35 ft setback with a slab.

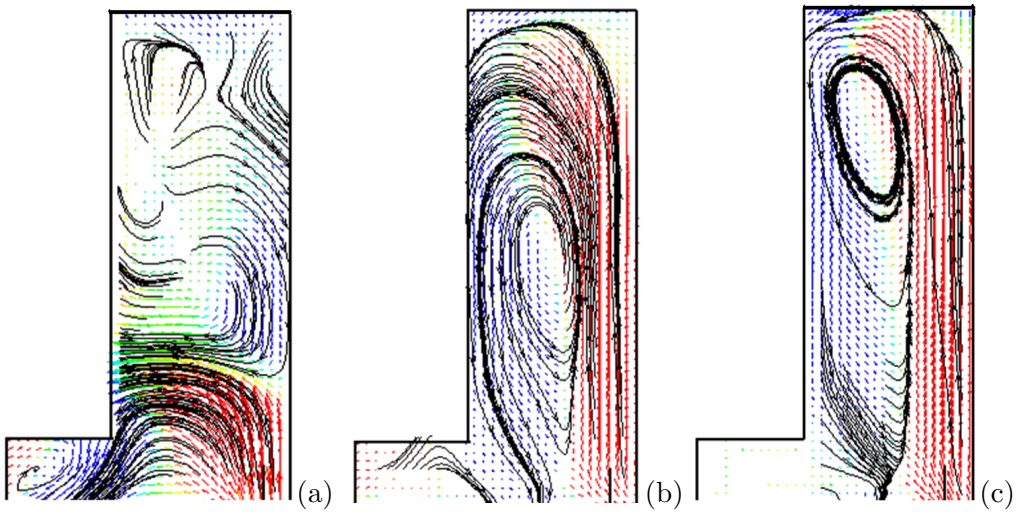

Figure 4.3: Streamlines from the PIV measurements for the simplified scrubber model for a 35 ft setback with a slab, $\boldsymbol{Q_s}$ / $\boldsymbol{Q_{in}}$ = 0.14 (a), 0.34 (b), 0.53 (c) respectively.

of 0.53.

In order to understand the effectiveness of the scrubber system with the miner machine in position, PIV measurements were conducted with the scrubber mounted on the continuous miner

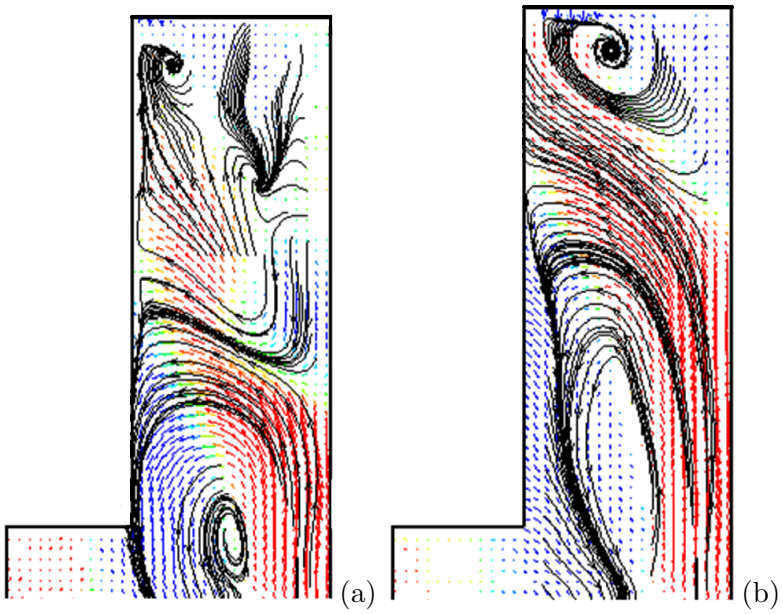

Figure 4.4: Streamlines from the PIV measurements with the machine mounted scrubber model for a 35 ft setback with a slab, $\boldsymbol{Q_s}$ / $\boldsymbol{Q_{in}}$ = 0.30 (a) and $\boldsymbol{Q_s}$ / $\boldsymbol{Q_{in}}$ = 0.53 (b).

model as shown in Figure 4.1b. Two different ventilation ratios of 0.30 and 0.53 were considered for this arrangement. The measurements were taken at a horizontal plane directly above the miner. Figure 4.4 shows the streamline plots for the ventilation ratios of 30% and 53%. Though the presence of the miner machine in the face area is an obstruction to the flow, with the scrubber system in position the amount of air delivered into the face area has improved.

4.3 Box cut with curtain setback of 60 ft

As shown previously scenario has had problems in bringing sufficient air to the face area. The scrubber system which proved very effective in providing good air distribution in the face area for 35 ft box cuts, was employed for this scenario too as seen in Figure 4.5 with encouraging results. From Figure 4.6 it was observed that the scrubber system has improved the air distribution in the face zone. This makes the 18.3 m (60 ft) deep cut mining scenario possible.

4.4 Summary

The scrubber system introduced basically for dust collection has proven to be a very useful tool in moving the air into the immediate face area. With a scrubber system for 18.3 m (60 ft)

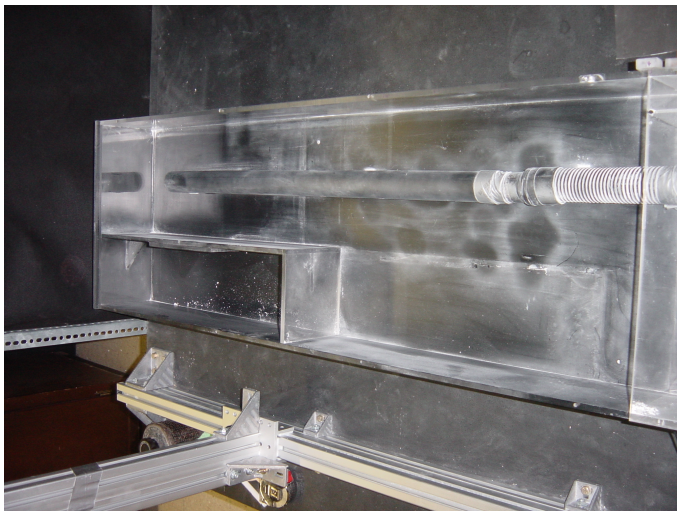

Figure 4.5: Scaled model with the simplified scrubber system for 60 ft deep cut.

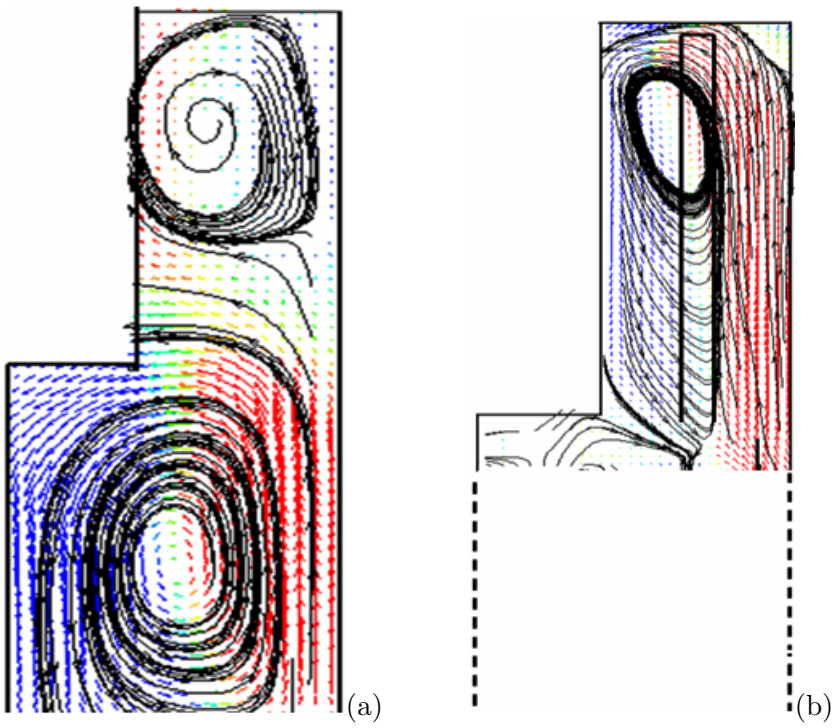

Figure 4.6: Streamlines from the PIV measurements with (a) and without the scrubber model (b) for a box cut with 60 ft setback.

deep cut mining scenario, the air distribution to the immediate face area has considerably improved making it a possible mining scenario. Also the flow ratio between the intake and scrubber is an extremely important factor, which can be controlled for optimization of face ventilation systems.

Chapter 5

Exhaust Ventilation System Results

5.1 Exhaust Scenarios

Blowing face ventilation systems with scrubber-equipped continuous mining machines are commonly used in U.S. underground coal-mines for extended cuts. This type of face ventilation system has been shown to be the most efficient if all the components of the system are working properly. However, in cases of scrubber failure or use of a continuous mining machine without scrubber or other mechanical face ventilation enhancing devices, the recommended blowing ventilation system must be replaced by exhaust ventilation system. A secondary study was performed for this ventilation system and some of those results are presented in this chapter.

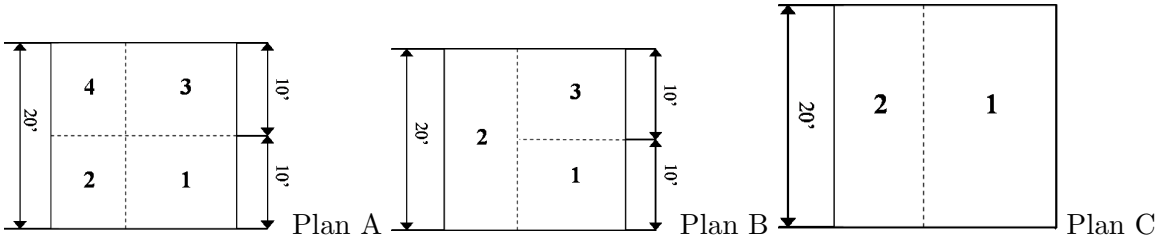

Figure 5.1: Three typical exhaust face ventilation arrangements for 6.1 m (20 ft) deep cuts. Plan "A" is examined in the current studies.

The characteristic parameters of these plans are as follows: (1) exhausting face ventilation systems; (2) cut depths of 20 feet; (3) the number of box (sump) cuts and slab cuts (cutting sequences) range from 2 to 4, (4) a line curtain air quantity of 2.1 m^3/s (4,300 cfm), and (5) the first cut will always be on the curtain side.

An experimental study demonstrating the Plan "A" as shown in Figure 5.1 using scaled model

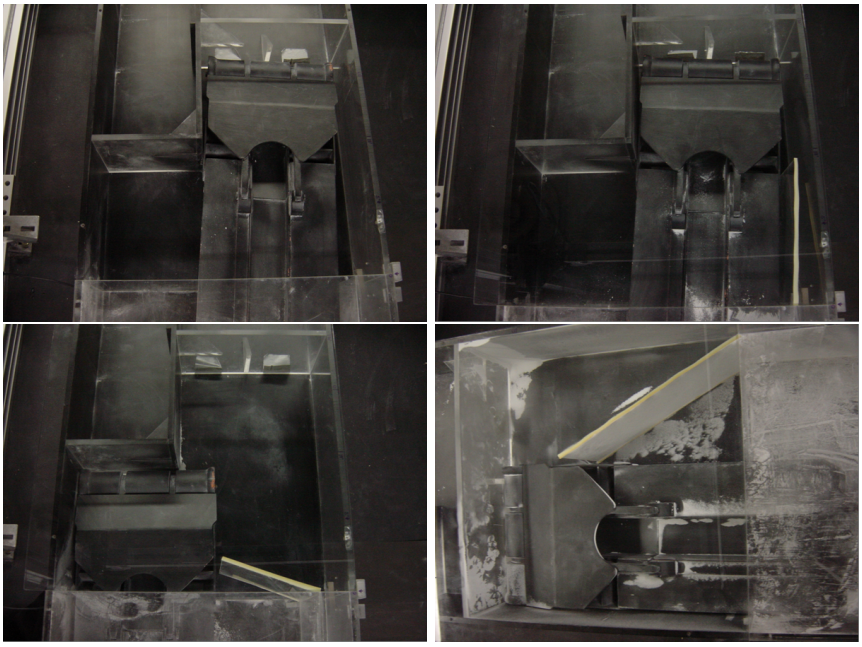

Figure 5.2: Scaled models with and without extensions for 3rd and 4th cuts.

equipped with PIV was performed. By utilizing the physical model of the face ventilation system, a number of different mining scenarios representing coal mining processes using continuous miners with an exhaust face ventilation system for 6.1 m (20 ft) depth extended cuts are examined. The pictures of the scaled physical model depicting these various mining scenarios are shown in Figure 5.2. For this particular study, as mentioned previously, the 4 cut sequence mining operation was adopted with three separate scenarios as discussed below.

5.1.1 Scenario #1

To be able to show the general flow behavior (distribution) in the face area for the exhaust face ventilation system, flow measurements were taken at the middle plane of the entry with no equipment. Figure 5.3 shows the velocity vectors in the face area just after the first cut and third cut were completed, respectively. As can be seen from these figures, most of the air is turning immediately back behind the curtain and only a limited amount is flowing towards the face. Nonetheless, whatever is getting into the face area is creating a large circulation region.

5.1.2 Scenario #2

A scaled model of a continuous miner, simulating a Joy Model 14 CM/10, was placed in the face area. Four different locations for the continuous miner, depending on cutting sequence, were

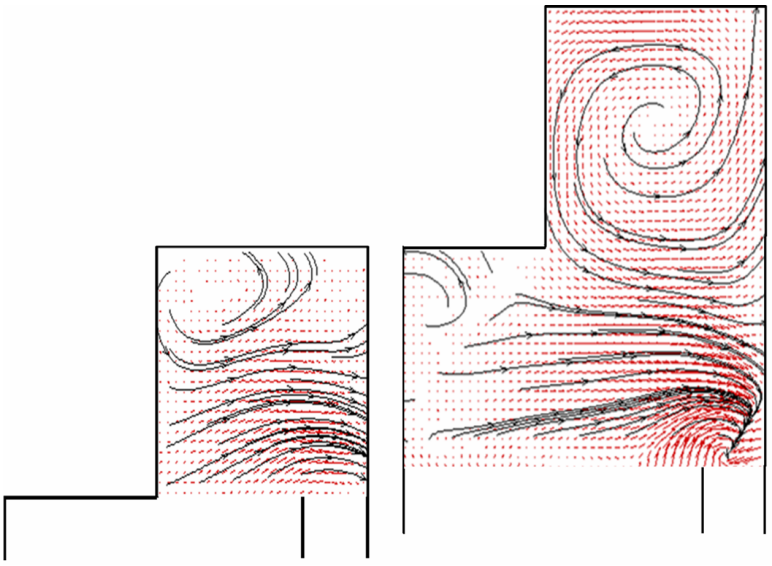

Figure 5.3: Velocity field with no miner; first (left) and third cut (right).

investigated. These locations were as follows : (i) halfway of the number 3 cut, (ii) end of the number 3, (iii) beginning of the number 4 cut, and (iv) end of the number 4 cut.

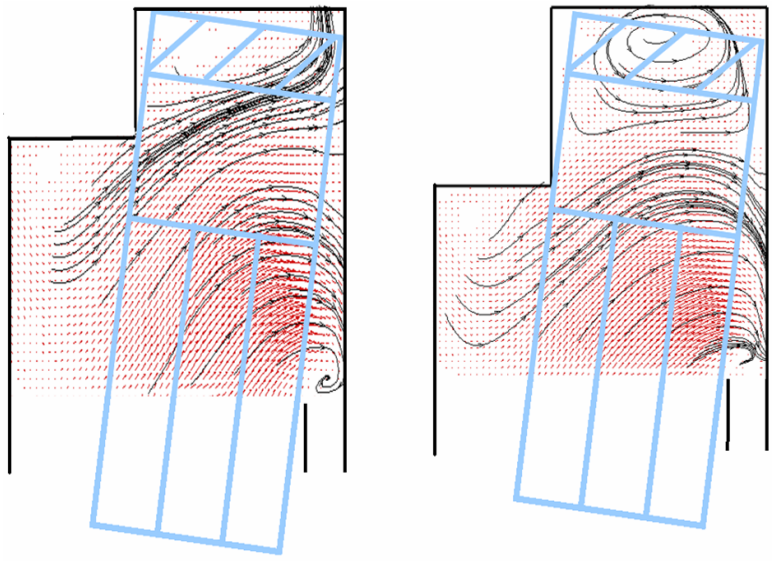

Figure 5.4: Halfway of third cut (left) and End of the third cut (right).

For all four arrangements the line curtain setback was 6.1 m (20 ft) with a quantity of air equivalent to 2.1 m^3/s (4,300 cfm). Figure 5.4 and 5.5 show the velocity vectors measured at the plane above the continuous miner, respectively, to the list above. Figure 5.3 (left) corresponds to

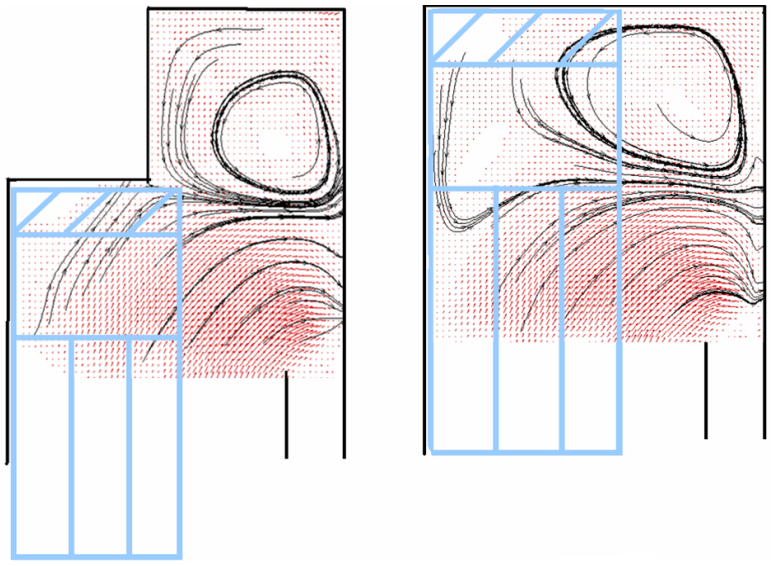

Figure 5.5: Starting (left) and ending (right) of the fourth cut.

5.4 (left); note that the presence of the miner changes the flow field, but not significantly. Again, as seen from all these figures, only a limited amount of air reaches the face area. This means that at the face where the cutting head of the continuous miner is located there is a lack of fresh air. Therefore, in such a case there is a question what can be done to improve this situation. Several ventilation enhancing devices include; (1) continuous miners with machine mounted scrubbers, (2) extendable line curtains/ flexible tubing, (3) jet fans, (4) spray-fans, and (5) a combination of these devices may be designed, tested and implemented. We examine the extendable line curtain below.

5.1.3 Scenario #3

To be able to show improvements in the flow distribution in the face area for the above tested scenarios, a well known practice of extendable curtains is implemented (see Figure 5.2) where it was applied to the same geometry and conditions tested in Scenario #2). A simple extendable curtain forces more air towards the cutting head of the continuous miner. On comparing Figure 5.4 (left) and 5.6 (left), we can see with an extendable curtain the penetration of air towards the face area has been significantly improved. Similarly comparing Figures 5.5 (left) and 5.7 (left) show improved air distribution with an extendable curtain.

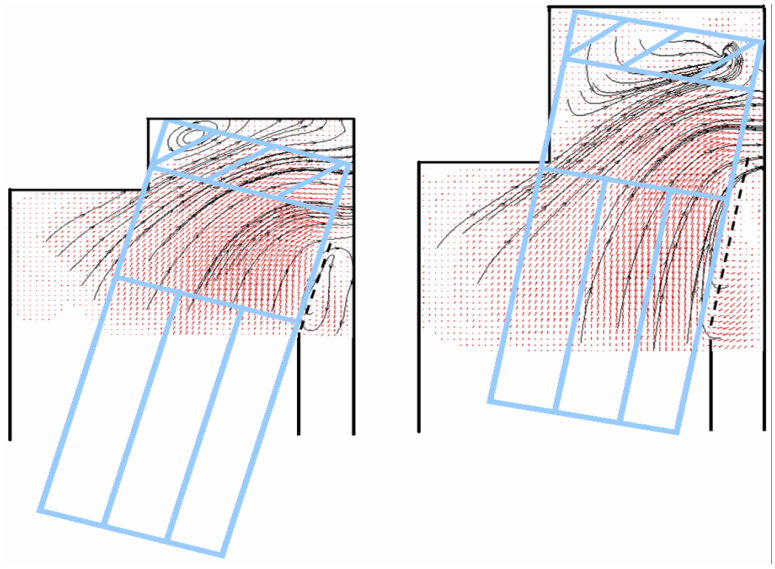

Figure 5.6: Starting (left) and ending (right) of the third cut with extendable curtain.

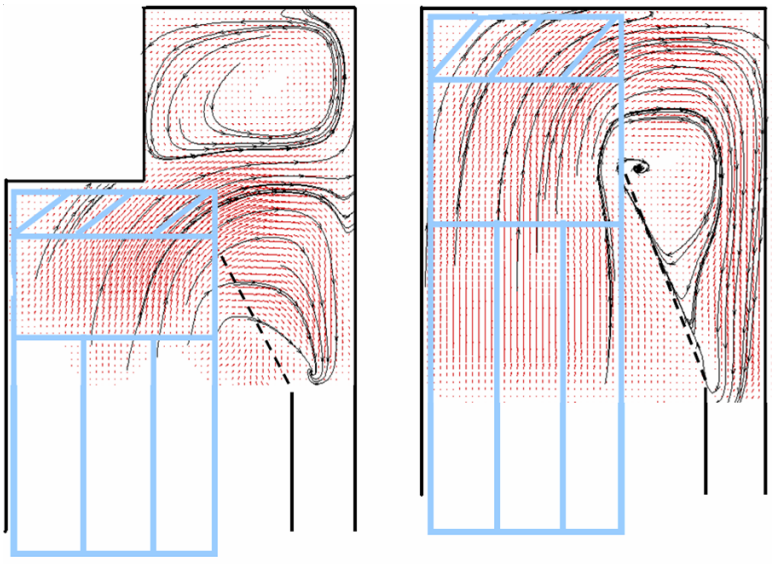

Figure 5.7: Starting (left) and ending (right) of fourth cut with extendable curtain.

5.2 Summary

Various mining scenarios for the exhaust ventilation system were studied. Considering the need to have sufficient air distribution in face area, exhaust ventilation system proved less effective than the blowing ventilation system. An exhaust ventilation system has very poor ventilation for 6.1 m (20 ft) curtain setback with no air enhancing devices in position. The presence of the miner machine worsened the ventilation in the face area. In order to improve the air distribution in the face area, extendable line curtains were employed in the system. These curtains greatly improved the ventilation.

Chapter 6

Additional Treatments

6.1 Full Size Measurements

To determine that the scaled physical model is a valid for the face ventilation systems, validation tests were performed in the full-size testing gallery at NIOSH Pittsburgh Research Center. The tests were conducted for two different entry widths of 13.5 ft and 16.5 ft, corresponding to 3.6 m (12 ft) and 6.1 m (20 ft) in the scaled model for a deep cut of 9.2 m (30 ft), respectively. The basic arrangement in the full-size gallery is as shown in Figure 6.1. The brattice line curtain is situated at the left hand side of the gallery as seen in Figure 6.2 and natural air ventilation was provided with the openings at the extreme end of the gallery. The slab was created by a flexible wall which can be removed and fixed as needed. The experiments were conducted with no equipment in position. The entry height of the testing gallery was about 2.14 m (7 ft).

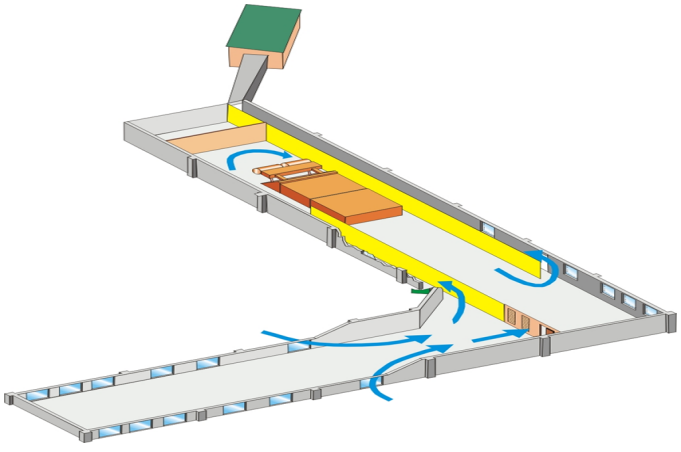

Figure 6.1: Schematic of the testing gallery at the NIOSH Research Center.

Figure 6.2: Testing Gallery at the NIOSH Research Center (a) and the camera setup(b).

The basic overall experimental setup is shown in Figure 6.2. The experimental setup consisted of a CCD camera on a trail of the gallery to the ceiling as shown in Figure 6.2b. The basic arrangement is shown in Figure 6.2a. This camera can be traversed both horizontally and vertically to study 3 ft by 3 ft interrogation region. The image captured by the camera is then processed in image capturing software to get the raw images. A Nd:YAG laser was used to illuminate the seeding particles. Using a double pulsed laser allows for easy control of the duration time between the pulses. The light sheet optics include both cylindrical and spherical lenses. The cylindrical lens diverges the laser beam into a sheet and the spherical lens controls the light sheet thickness which is approximately 1 mm at the focal length. The laser sheet was adjusted to hit at a height of 1 foot from the floor. The interrogation region to be observed was 3 ft by 3 ft in area. Baby powder was used as a seeding for the flow. The seeding was kept in a cylindrical container and was forced out using pressurized air. A tubing with multiple openings was used to release the seeding into the flow.

Figure 6.3 represents a series of raw images for an entry of 13.5 ft which corresponds to the scenarios of box cut 9.1 m (30 ft) depth. As you can see from the figures, the separation behavior resembles very much what was observed in the scaled physical model. The flow clearly separates at a distance of 12 ft from the brattice line curtain. The fourth interrogation region shows the separation taking place. This flow is called the "Primary flow" as most of it separates and returns through the exhaust. The minor amount of flow which flows towards the face area in an opposite direction is called the "Secondary flow." On the other hand from Figure 6.4, for an entry width of 16.5 ft which corresponds to a slab cut of 6.1 m (20 ft) wide and 9.1 m (30 ft) depth, the flow has

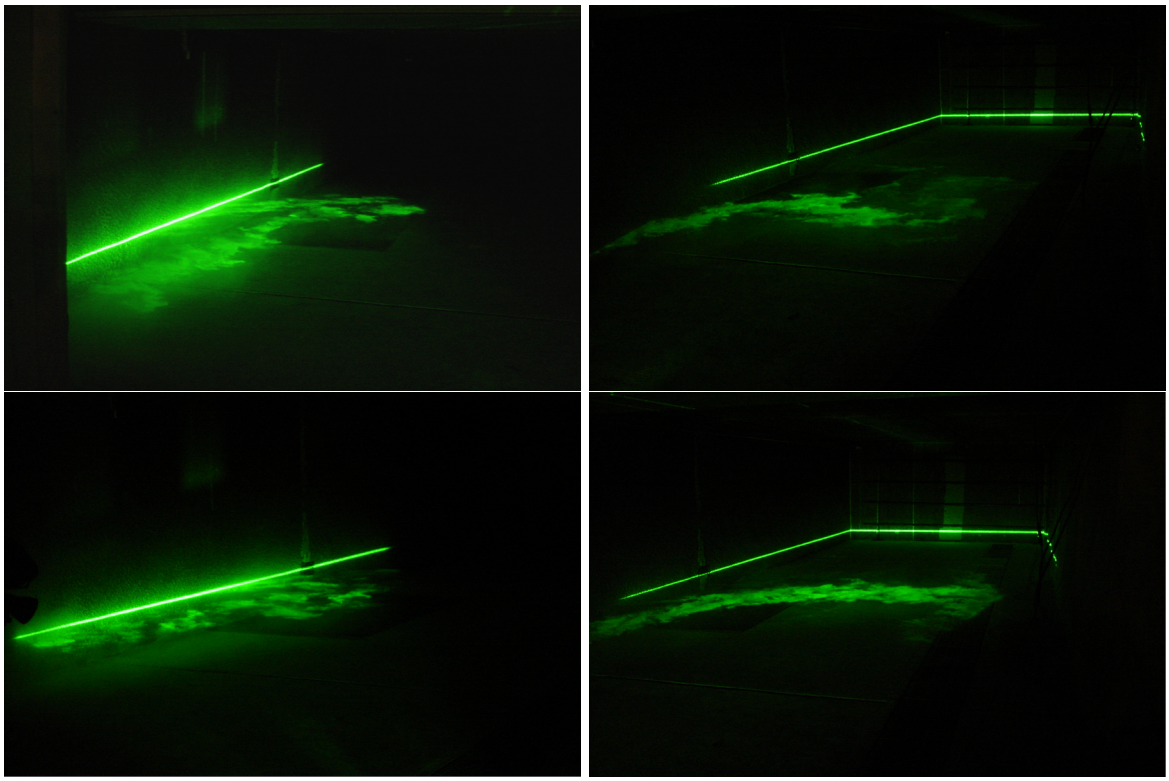

Figure 6.3: Raw Images for an entry of 13.5 ft.

penetrated all the way until it reaches the face with no secondary flow patterns. This behavior is very similar to the one which was observed in the scaled physical model.

Figure 6.5a shows the locations were the data was taken in the full-size laboratory and Figure 6.6 shows the two-dimensional flow distributions (velocity vectors) for 13 ft and 16 ft for an interrogation region of 3 ft by 3 ft. Figure 6.5c shows the velocity vectors for the scaled model and Figure 6.5b full size testing gallery at NIOSH for comparison purposes. Both tests showed the same (unexpected) behavior. (Note that since the time scales are much larger in the full scale scenario, fluctuations in the flow field did not provide as clear as a picture as in the model). The flow was very similar in its behavior in the scaled model and full size gallery. After this encouraging result, it was confirmed that scaled physical models can be used for validation of face ventilation plans and in aid in the plan approval process.

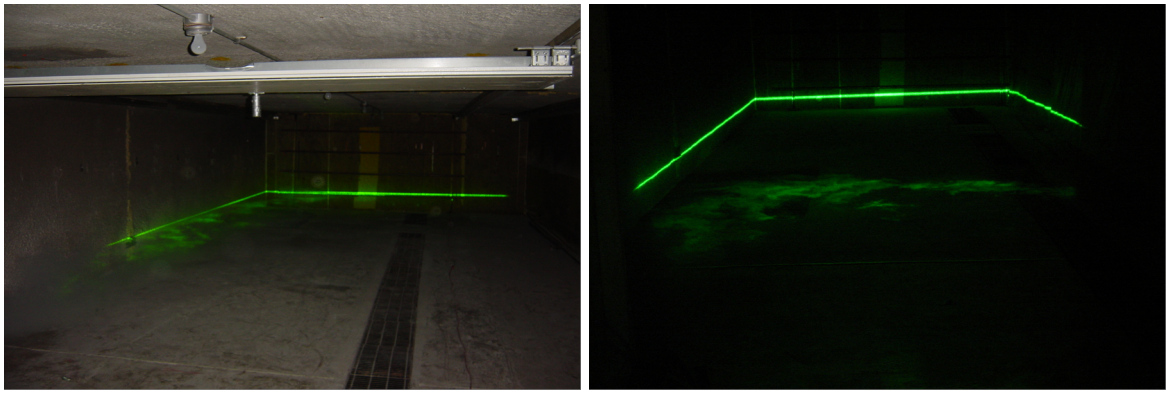

Figure 6.4: Raw Images for an entry of 16.5 ft.

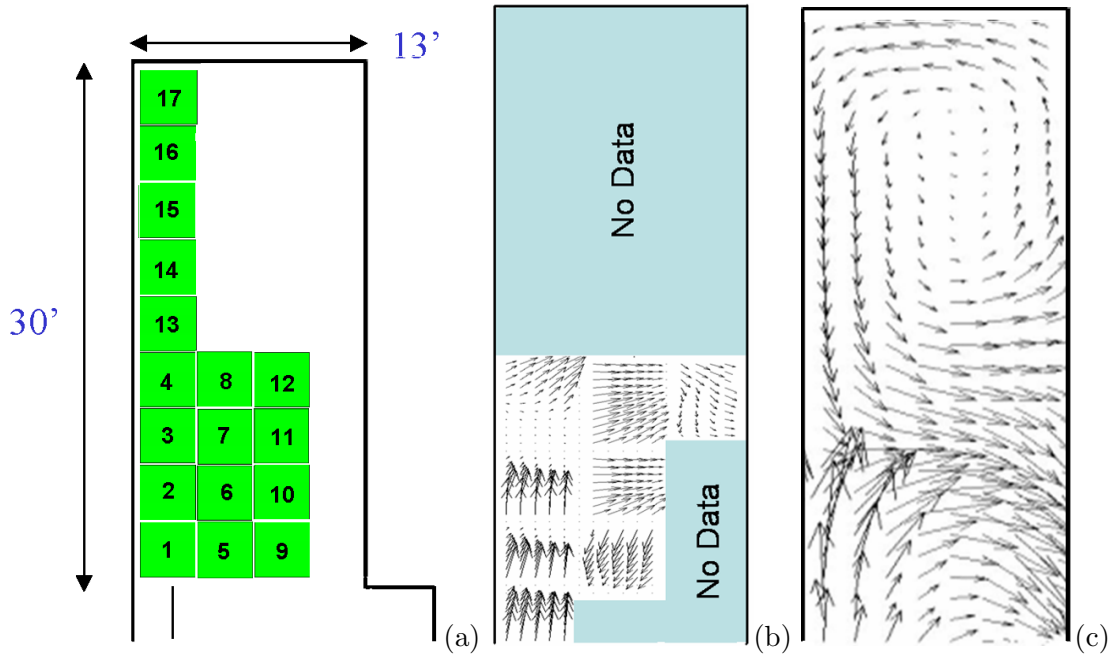

Figure 6.5: Areas where the data was taken (a) and velocity vectors for the full-size test (b) and scaled model (c).

6.2 CFD Calculations

6.2.1 Introduction

Several scenarios are explored to compare the CFD results to experimental data taken with PIV. Commercial CFD packages Fluent and CFX were used to predict these results Brown. J (2003). The objective was to utilise the software's many features to obtain accurate prediction of the onset separation that occurs during three of the four scenarios. This separation of the flow

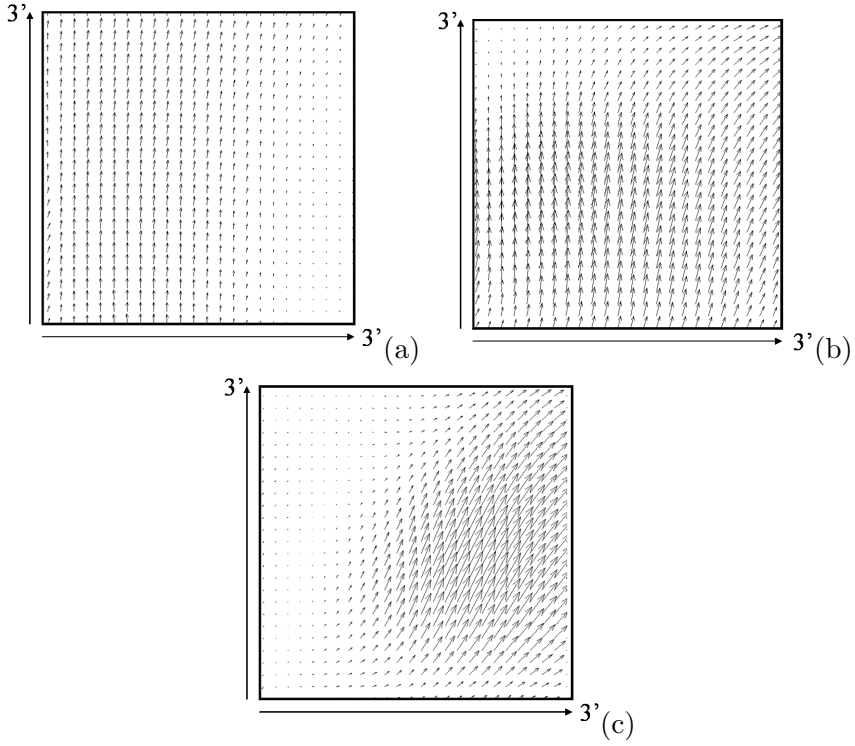

Figure 6.6: Velocity vectors for one interrogation region for entry widths of 13 ft at three different locations; Location 1 (a), Location 3 (b), Location 4 (c). Note that these locations correspond to the locations in Figure 6.5a.

prevents proper ventilation near the face and allows the accumulation of methane at the cutting face. Also these CFD packages can help to study more complex scenarios which are not possible to achieve by experimentation alone. But for the approval of these CFD results, validation with the experimental data is very essential. The following sections here show the comparison between the experimental data and the CFD data.

6.2.2 Comparison of CFD results with PIV for general geometries

30 Foot Box Cut

In this scenario an onset separation develops only a few feet downstream from the end of the curtain at the beginning of the slab. This separation produces a low velocity recirculation of air in the face area. Comparing the results (Wala et al., 2004) as shown in Figure 6.7 we see that both Fluent and CFX correlate well with the experimental data for moderate grids. The onset separation and the recirculation of air in the face area were very similar with Fluent and CFX

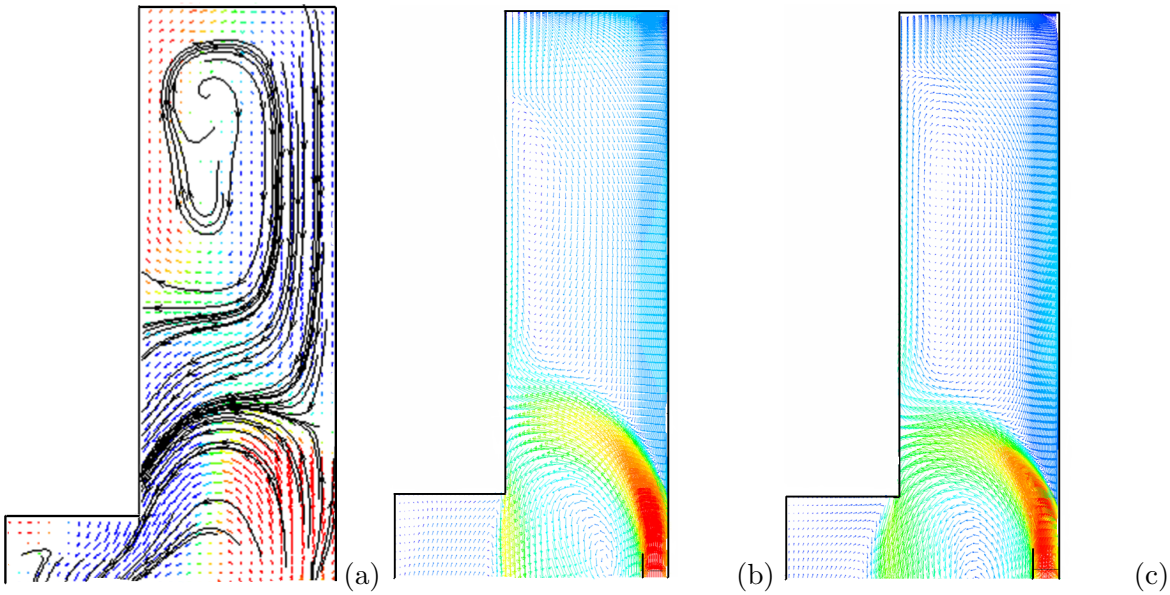

Figure 6.7: Velocity vectors from PIV (a), Fluent (b) and CFX (c) for 30 ft box cut using a moderate grid.

softwares. However CFX does not predict the separation correctly for coarse and fine grids. So from the results we see that the coarse grid solutions for both Fluent and CFX predict similar flow behavior as observed in experimental plots for this scenario. Comparing the results with the experimental results, one can see that Fluent predicts the desired characteristics independent of grid density. CFX results show that grid independence has not been achieved.

30 Foot Slab Cut

In this scenario no onset separation occurs as the flow penetrates to the face area. Simulations performed for this scenario helped to test the codes ability to decipher the difference between flows with separation and without separation. The results were considered for three grid sizes of coarse, moderate and fine. Results from Fluent showed similar flow patterns as observed from PIV for all the grid sizes. However for CFX, from the Figure 6.8 for moderate grid size, we see that the jet separated a little early. It did not exactly traverse the face as it did in the plot using Fluent. The jet was also wider on reaching the face area. Though it did not exactly correlate well with the velocity vectors from Fluent but the results from CFX predicted similar flow behavior with a moderate grid. With coarse and fine grids, the jet spread wider at about 3 ft from the face area loosing its dynamic energy, whereas in CFX, had a much narrower jet going to the face area. For the case with fine grid, Fluent had a much dispersed jet as opposed to CFX. But noticing for all

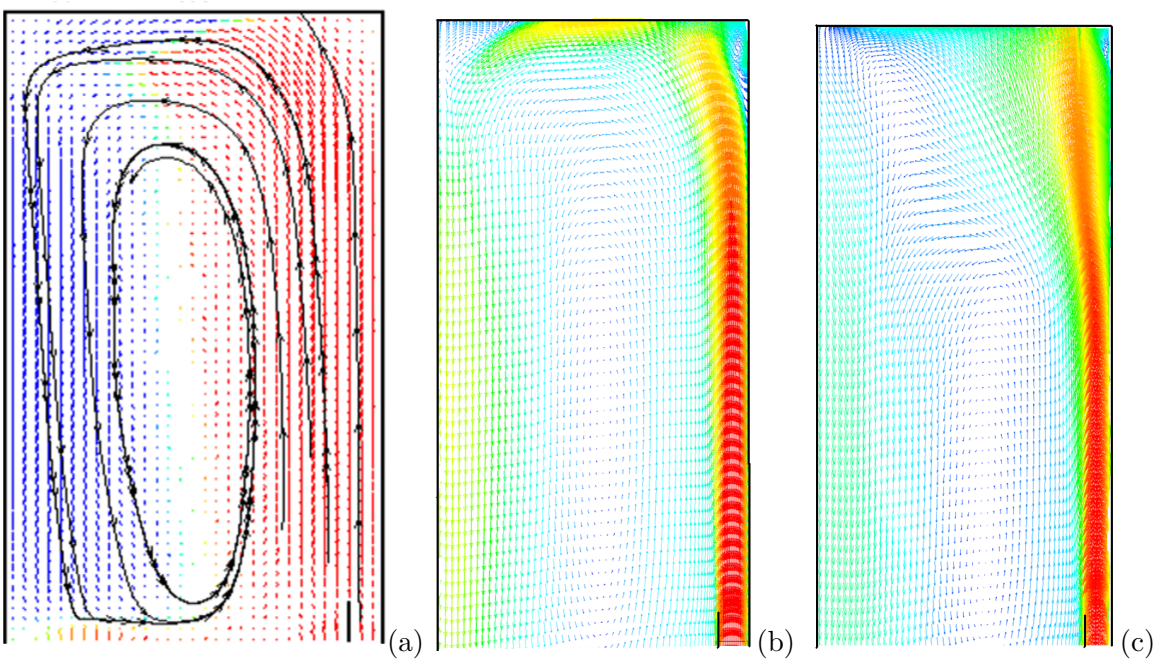

Figure 6.8: Velocity vectors from PIV (a), Fluent (b) and CFX (c) for 30 ft slab cut using a moderate grid.

the three grid levels the flow carries to the mine face before turning, one can confirm that both codes predict a similar grid independent solution.

60 Foot Box Cut

In the 60 foot box cut scenario onset separation occurs at the beginning of the slab as shown in Figure 6.9 at the exact same location shown for 30 foot box cut. Both the codes predicted similar results as PIV for all the grid sizes except for minor discrepencies. From Figure 6.9, we see that both CFX and Fluent codes predcited the exact nature in the region of separation. However, at the recirculation region near the face, we observe a presence of a small vortex at the extreme left hand corner for Fluent, but in the case of CFX, this was moved down a little bit. Also for the cases with coarse and fine grids showed similar results with some minor differences in the recirculation region. The CFD codes did not have a problem in predicting the similar behavior as experimental data and have prove to be useful in predicting results for different cases for this scenario in the future. Therefore, one can claim that the grid-independent solution generated by both the codes is accurate for this scenario.

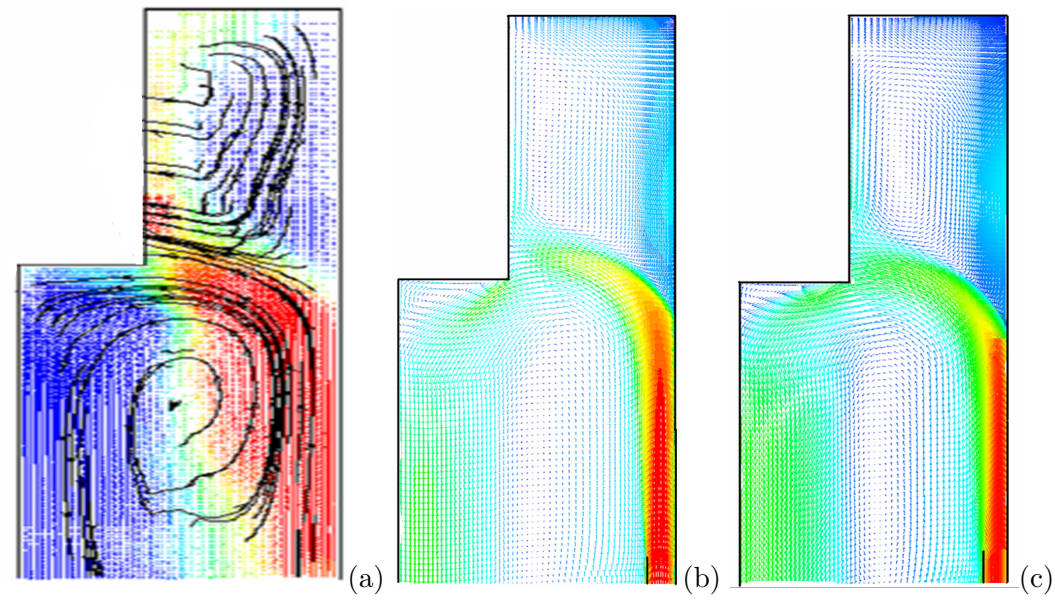

Figure 6.9: Velocity vectors from PIV (a), Fluent (b) and CFX (c) for 60 ft box cut using a moderate grid.

60 Foot Slab Cut

For this scenario from the PIV results, we observe a late separation that occurs unlike the 30 foot slab cut scenario where the flow was carried to the face area. Figure 6.10 shows the comparison between the PIV, Fluent and CFX results. However, both Fluent and CFX codes could not predict the similar behavior and have failed in studying this particular scenario. The codes were run using three different grid sizes and yet none of them converged and produced accurate results. Both the codes showed that the flow was carried to the face area. Due to the highly unstable nature of the flow, an accurate steady-state simulation of flow structure was not feasible. The codes inability to generate a converged solution yielded variation in the results. One suggestion may be to approach the problem from a transient standpoint to capture any oscillations that may occur in the flow. So this case needs further study before results can be utilized as a reliable design tool.

6.2.3 Comparison of the CFD results with the Scrubber Ventilation System

In this section, a cylindrical scrubber was inserted into the 30 ft box cut geometry and the results were compared with the PIV data. The scrubber mass flow ratio is normalized by the mass flow at the inlet, or behind the curtain. Four different mass flow ratios of 0.2, 0.3, 0.7 and 1.0 were considered. From Figures 6.11, 6.12 and 6.13, we see results for the ventilation ratios of 0.2, 0.3

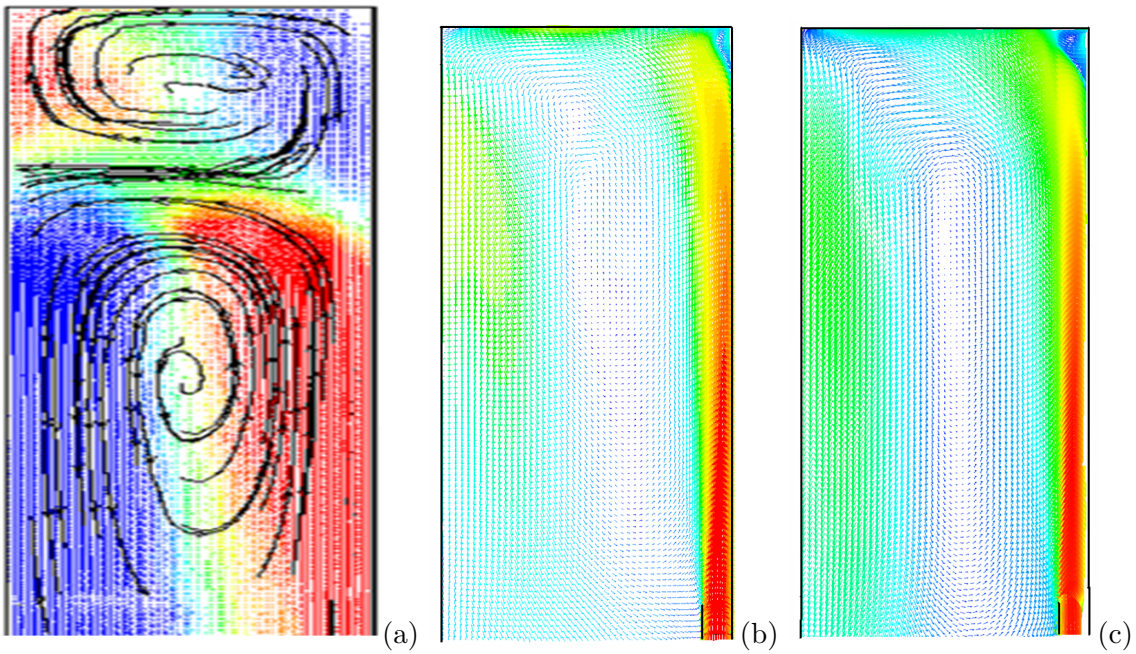

Figure 6.10: Velocity vectors from PIV (a), Fluent (b) and CFX (c) for 60 ft slab cut using a moderate grid.

and 0.7. From Figure 6.11, for a ventilation ratio of 0.2, Fluent could not predict the separation region as PIV. The onset separation was deeper than the PIV data where the flow separated immediately. The path lines shown by Fluent show this nature more clearly. Figure 6.12 shows the comparison between the PIV data and the Fluent data for a ventilation ratio in the range of 0.35. The ventilation ratios considered for PIV was 0.34 and for Fluent was about 0.4. We see that PIV showed almost an unseparated flow behavior. But Fluent showed flow separation far down from the face even though it had a higher ventilation ratio. From Figure 6.13, the ventilation ratio for the PIV data was about 0.53 and for Fluent was about 0.7. Both the plots showed similar flow characteristics. From all these results, however, we can say that Fluent predicted similar behavior for most of the cases but still needs more rigorous validation for its engineering use in ventilation design.

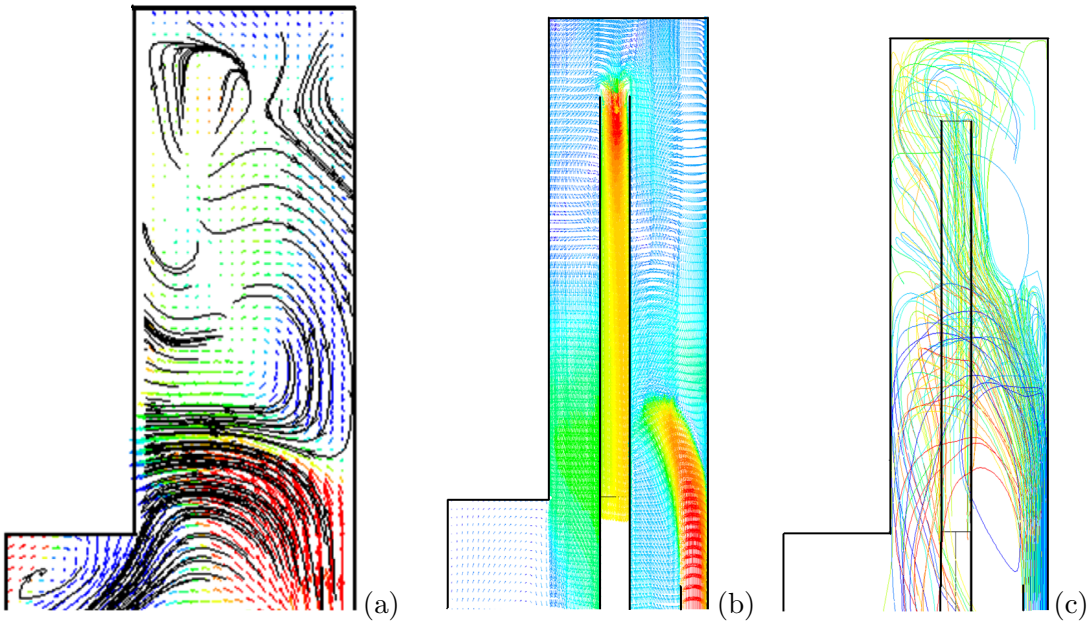

Figure 6.11: Streamline plot from PIV (a), velocity vectors (b) and path lines (c) from Fluent with $\boldsymbol{Q_s/Q_{in}}$ in the range of 20%.

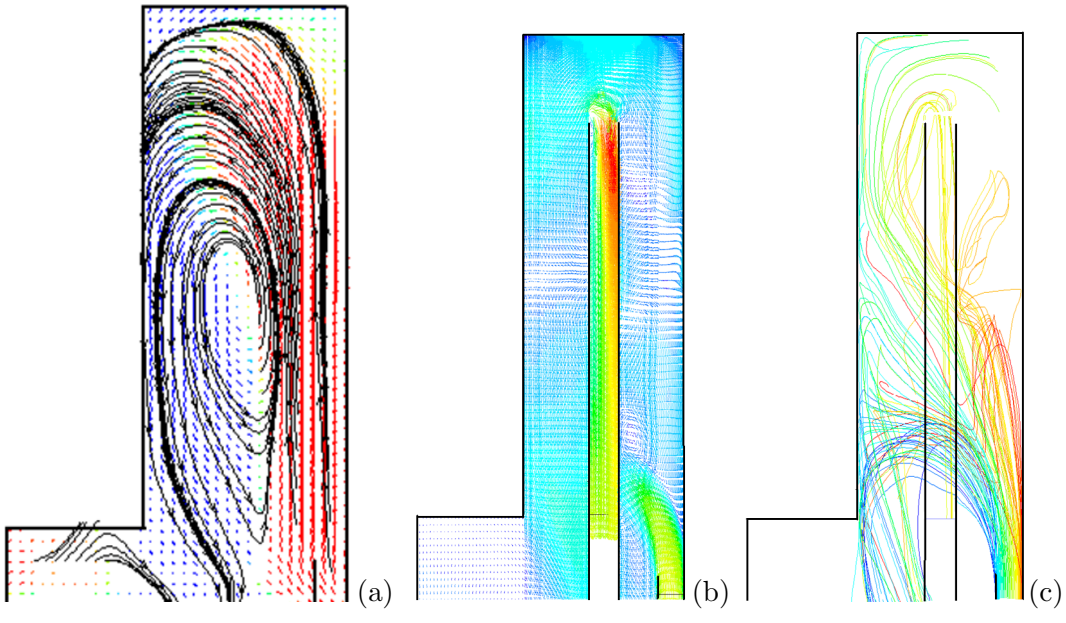

Figure 6.12: Streamline plot from PIV (a), velocity vectors (b) and path lines (c) from Fluent with $\boldsymbol{Q_s/Q_{in}}$ in the range of 35%.

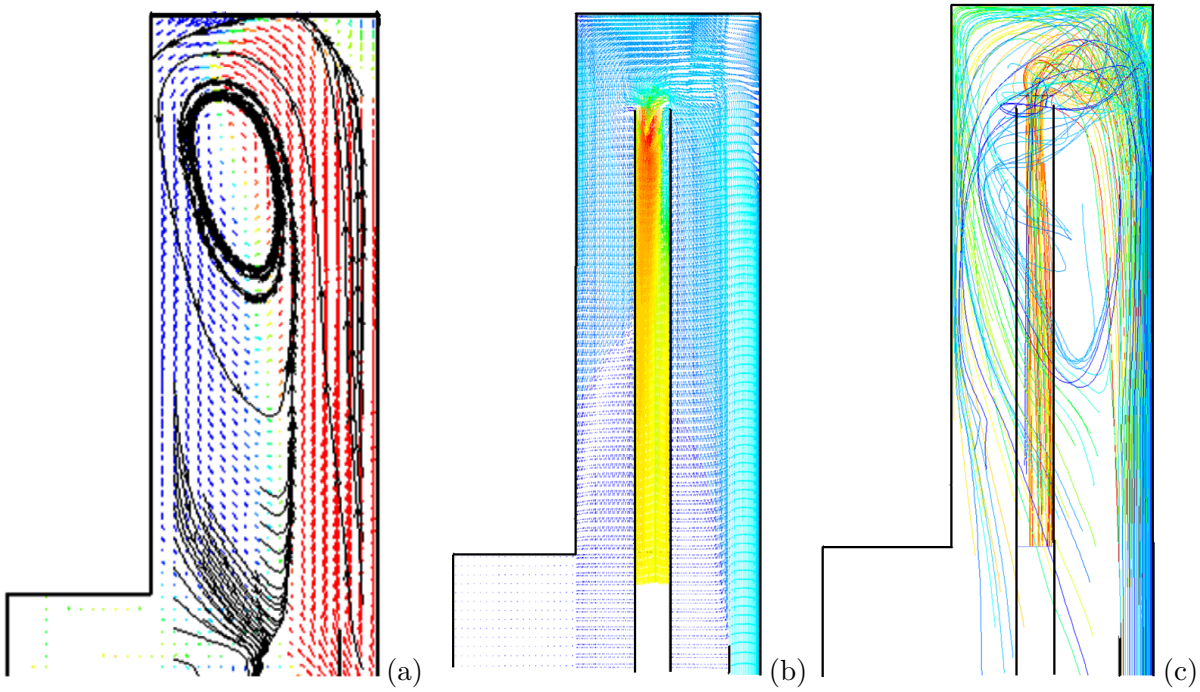

Figure 6.13: Streamline plot from PIV (a), velocity vectors (b) and path lines (c) from Fluent with $\boldsymbol{Q_S/Q_{in}}$ in the range of 70%.

Chapter 7

Conclusions

Face ventilation of underground coal mines is very important for the health and safety of the miners. The present thesis discussed the mining scenarios which have the face ventilation problems and also studied this complex flow behavior and the effect of various geometric and flow parameters to have good air distribution in the face area for improved ventilation. For most of the studies performed, the presence of the miner machine and introduction of methane gas in the face area were not considered. Studies considering these two parameters will be performed in future.

The various scenarios which were studied included slab and box cuts for two different depths of 9.1 m (35 ft) and 18.3 m (60 ft). The effect of various geometric and flow parameters such as entry width, curtain widths, entry heights and different inlet flow velocities was studied. Of all these parameters, the entry widths and the curtain widths had the largest effect the flow behaviors. A critical width of 4.9 m (16 ft) was found to have no flow separation. From the results curtain width of 0.306 m (1 ft) was helpful in increasing the dynamic velocity of the air flow and in bringing the flow to the face area. Study concerning the wall bounded jet characteristics was performed. Jet spreading angles 'β' and virtual origins 'x_p' were calculated for different geometries showing that variation of face zone widths '$\boldsymbol{W_f}$' and curtain widths '$\boldsymbol{W_c}$' considerably affect the flow. As the $\boldsymbol{w_f}$ was increased from 3.6 m (12 ft) to 6.1 m (20 ft) for a 9.1 m (30 ft) deep cut, the spreading of the jet became narrower with β values reducing from 35° to 8.132°. Also as the $\boldsymbol{W_c}$ was decreased from 1.225 m (4 ft) to 0.306 m (1 ft), the jet spreading angles reduced from 35° to 5.7°, thus making the flow more narrower.

The implementation of scrubber into the system considerably helped in bringing more air to the dead end on the mine entry. Various ventilation ratios $\boldsymbol{Q_s/\ Q_{in}}$ ranging from 0.14 to 0.53 were studied. From the results, it was understood that the penetration of the flow into the mine heading increased with the ventilation ratios. Scrubber system helped to have have good air distribution in

the face area with the miner machine present which is a major obstruction to the flow.

The full scale study was conducted at the full-size gallery at NIOSH to validate the scaled physical model. The full scale data correlated well with the experimental data on the physical model making the scaled physical model a valid tool in using for the face ventilation studies.

Studies concerning the introduction of methane and placement of miner machine, which complicate the flow, are to performed using Computational Fluid Dynamics (CFD) in future. Though the experimental analysis from this thesis has given some confidence in using CFD in future with minimal errors, it still needs extensive validation to be approved and used by the mining industry.

Appendix A

Matlab Code

```
function mineminer
% program to average mining data sets
% use for processed sets such as 10.18.01
% geometry 16

%run number
clc;
run=6
%data set -- set this to 0 if file has format tenXXX.XXX instead of tenXXX-X.XXX
set=0
%height of laser sheet, 1 or 2
%number of tensor files
ntot=51 %nini=1
%ntot2=ntot; ntot=ntot-nini+1;
set=1;

%set base path of files
basepath='G:\Thesis\Different Curtain Widths\New Correct Data\07.08.03\tensors\'
%runc=int2str(run);
%basepath=strcat(basepath1,run,'\');

%conversion info - spatial and temporal scales to give units in m/s
scale=28 %pixels/cm
```

```
pulse=200     %pulse timer in microseconds

%conversion factors to m/s
convel=(scale*100*pulse/1000000);
convor=(pulse/1000000);

%check array sizes?
[nx,ny]=arraychecker(run,set,1,basepath)
%or set size of arrays manually
%nx=62;ny=62;

%create empty arrays
uav=zeros(ntot,nx,ny);
vav=zeros(ntot,nx,ny);
vortav=zeros(ntot,nx,ny);
contav=zeros(ntot,nx,ny);
un=zeros(nx,ny);
vn=zeros(nx,ny);
vorn=zeros(nx,ny);
conn=zeros(nx,ny);
corn=zeros(nx,ny);
ctr=zeros(nx,ny);
urms=zeros(nx,ny);
dvdxn=zeros(nx,ny);

%characteristic velocity based on 5400 fpm (~30 m/s)
uf=1;
cfx=58;

%read in data files
for i=1:ntot
    [u,v,vort,cont,corr,dvdx]=minefunc(run,set,i,basepath);
    un=u+un;
```

```
    vn=v+vn;
    vorn=vort+vorn;
    conn=cont+conn;
    corn=corr+corn;
    %figure(i)
    %contourf(vort,50),axis off,axis ij,axis equal
    uav(i,:,:)=u;
    vav(i,:,:)=v;
    vortav(i,:,:)=vort;
    contav(i,:,:)=cont;
    dvdxn=dvdxn+dvdx;
        for j=1:nx
        for k=1:ny
            if v(j,k) < 0
                ctr(j,k)=ctr(j,k)+1;
            end
        end
    end
end

%pause

fprintf('\nThinking')

%caclulate averages
un=un/ntot;
vn=vn/ntot;
vorn=vorn/ntot;
conn=conn/ntot;
corn=corn/ntot;
dvdxn=dvdxn/ntot;
ctr=ctr/ntot;
```

```
%scale data
un=un/convel;
vn=vn/convel;
vorn=vorn/convor;
uav=uav/convel;
vav=vav/convel;

%calculare rms turbulence
for j=1:nx
    fprintf('.')
        for k=1:ny
            dum1=0; dum2=0; dum3=0;
            for i=1:ntot
                dum1=sqrt(un(j,k)^2+vn(j,k)^2);
                dum2=sqrt(uav(i,j,k)^2+vav(i,j,k)^2);
                dum3=(dum1-dum2)^2+dum3;
            end
            urms(j,k)=sqrt(dum3)/ntot;
        end
    end

%skin friction coef.
mu=0.0000185;
shear=mu*dvdxn;
cf=shear/(0.5*1.23*uf^2);
%cf=cf(1,12:82);
size(cf)

% PLOTTING

offset=0;
xllim=offset;
yllim=offset;
```

```
xulim=nx-offset;
yulim=ny-offset;

% %set edge regions to zero if need be
  un(:,1)=0; vn(:,1)=0; vorn(:,1)=0;
  un(:,2)=0; vn(:,2)=0; vorn(:,2)=0;
  un(1,:)=0; vn(1,:)=0; vorn(1,:)=0;

  for i=1:nx
      for j=1:ny
         mag=sqrt(un.^2+vn.^2);
          if mag(i,j) > 0.565*max(mag)
              un(i,j)=0;
              vn(i,j)=0;
          end
      end
  end


%new colormap
jet2=abs(jet-1);
mag=sqrt(un.^2+vn.^2);
%mag=un;

%vertices for patch command for slab (if needed)
xc=9; yc=27;
x1=[10 10 31 31 1 1];
y1=[62 39 39 13 13 62];
x2=[40 50 50 40];
y2=[49 49 1 1];
x3=[0 50 50 0];
y3=[1 1 -1 -1];
```

```
splash=strcat(': miner Run-',int2str(run));%,', Level-',int2str(set));

% PLOTS
figure(1);
colormap jet;
contourf(mag,50),axis equal,axis off,axis([xllim xulim yllim yulim]),
title(strcat('Velocity',splash)),axis ij,shading flat;
colorbar; %gtext('m/s');
hold on;
quiver(un,vn,3,'k'),axis equal,axis([xllim xulim yllim yulim]),axis ij,axis off
skip=1;
quiver(un(1:skip:nx,1:skip:ny),vn(1:skip:nx,1:skip:ny),2,'k'),axis equal,
axis([xllim xulim yllim yulim]),axis ij,axis off
patch(x1,y1,'k'); %patch(x2,y2,'k'); patch(x3,y3,'k');% hold off;

figure(2)
contourf(un,25),axis ij,axis equal, shading flat

figure(3)
contourf(vn,25),axis ij,axis equal, shading flat

figure(4);
colormap jet;
contour(vorn,50),axis off, axis equal,axis([xllim xulim yllim yulim]),
title(strcat('Vorticity',splash)),axis ij,shading flat;
colorbar; %gtext('s^{-1}');
patch(x1,y1,'k'); patch(x2,y2,'k'); patch(x3,y3,'k');

figure(5);
colormap jet;
contourf(ctr,50),axis off,colorbar,axis equal,axis([xllim xulim yllim yulim]),
title(strcat('FFP',splash)),axis ij,shading flat;
colorbar;
```

```
patch(x1,y1,'k'); patch(x2,y2,'k'); patch(x3,y3,'k');

figure(6);
colormap jet;
contourf(urms,50),axis off, axis equal,axis([xllim+2 xulim-2 yllim yulim]),
title(strcat('RMS Velocity',splash)),axis ij;,shading flat;
colorbar;
patch(x1,y1,'k'); patch(x2,y2,'k'); patch(x3,y3,'k');

figure(7);
colormap jet;
contourf(conn,50),axis off, axis equal,axis([xllim xulim yllim yulim]),
title(strcat('Continuity',splash)),axis ij;
colorbar;
patch(x1,y1,'k'); patch(x2,y2,'k'); patch(x3,y3,'k');

figure(8);
colormap jet;
contourf(corn,[0 .1 .2 .3 .4 .5 .6 .7 .8 .9 1.0]),axis off, axis equal,
axis([xllim xulim yllim yulim]),
title(strcat('Avg. PIV Correlation',splash)),axis ij;
colorbar;
patch(x1,y1,'k'); patch(x2,y2,'k'); patch(x3,y3,'k');

ddv=1;

for cross=30:-10:20
vllim=-5;
vulim=5.0;
xllim=10;
xulim=50;

[vmax1,xmax1]=max(-vn(cross,:))
```

```
for i=xmax1:-1:1
    if -vn(cross,i)<vmax1./2
        vmaxh1=-vn(cross,i)
        xmaxh1=i
    break
end

end

 figure(9);
 plot(-vn(cross,:),'ro-')
 hold on
 plot(xmax1,vmax1,'b.','Markersize',25)
 plot(xmaxh1,vmaxh1,'c.','Markersize',25)
 hold off
 axis([xllim xulim vllim vulim]);

% pause

vllim=-5;
vulim=5.0;
xllim=10;
xulim=50;

 for k=1:ntot

 [vmax1,xmax1]=max(-vav(k,cross,:))
 for i=xmax1:-1:1
     if -vn(cross,i)<vmax1./2
         vmaxh1k=-vav(k,cross,i)
         xmaxh1k=i
         xmhi(i)=i
         crossi(i)=cross
```

```
    break
    end
end

end

figure(10);
plot(-squeeze(vav(k,cross,:)),'ro-')
hold on
plot(xmax1,vmax1,'b.','Markersize',25)
plot(xmaxh1k,vmaxh1k,'c.','Markersize',25)
hold off
axis([xllim xulim vllim vulim]);
% ylabel('Velocity in direction of the Face');
% xlabel('Width across face');

pause

figure(11)
skip=1;
quiver(un(1:skip:nx,1:skip:ny),vn(1:skip:nx,1:skip:ny),4,'k'),axis equal,
axis([xllim xulim yllim yulim]),axis ij,axis on
% title('Curtain Width of 2ft');
hold on;
plot([0 50],[cross cross],'r-')
plot(xmax1,cross,'b.','Markersize',25)
plot(xmaxh1,cross,'c.','Markersize',25)

figure(12)
skip=1;
quiver(un(1:skip:nx,1:skip:ny),vn(1:skip:nx,1:skip:ny),4,'k'),axis equal,
axis([xllim xulim yllim yulim]),axis ij,axis on
hold on
```

```
plot(xmaxh1,cross,'r-.',xmaxh1,cross,'c.','Markersize',25)

xmh(ddv)=xmaxh1;
crs(ddv)=cross;

ddv=ddv+1;

end

% figure(8)
% hold off
% figure(9)
% hold off
% figure(10)
% hold off
% figure(11)
% hold off
% figure(12)
% hold off
% figure(11)

 %save data
save(strcat(basepath,'result',int2str(run)),'un','vn','vorn','ctr')

return;
%end of main routine
%%%%%%%%%%%%%%%%%%%%%%%%%%%%%%%%%%%%%%%%%%%%%%%%%%%%%%%%%%%%%%%%%%%%%%%%%%%%%%%
function [e1,e2,vorticity,continuity,corr,dudy,dvdx]=minefunc(run,set,batch,basepath)
% MATLAB Script to read WALPT data and image files.
% Jamey Jacob, Jan. 18 2000
% Version 1.1, last modified Feb. 15, 2000
% Miner version May 30, 2001 - only data read
% For use with MATALB release 11 (5.3)
```

```
% Ticker will not work with older versions (see "movie")
% jdjacob@uky.edu

% setflag=set;
% set=int2str(set);
run=int2str(run);
bat=int2str(batch);

%run='2b11';

% file and path names
%run='8';lptfile=strcat('tensor',run,'.out');
lptima1=strcat('image',run,'a.lpt');
lptima2=strcat('image',run,'b.lpt');
if batch == 0,
    if setflag == 0
        lptfile=strcat('ten',run,'.out');
    else
    lptfile=strcat('ten',run,'-',set,'.out');
    end
u_infinity=0;
v_infinity=0;
   details=''
else
if batch < 10
  bat=strcat('.00',bat);
else
if batch < 100
    bat=strcat('.0',bat);
else
  bat=strcat('.',bat);
      end
   end
```

```
%    if setflag == 0
       lptfile=strcat(run,bat);
%    else
%      lptfile=strcat(run,'_',set,bat);
%     end
    lptfile=strcat(run,bat);
    lptima1=strcat('image1.lpt');lptima2=strcat('image2.lpt');
     u_infinity=0;
 v_infinity=0;
end

%SET PATHS AND FILE NAMES
%path=strcat(basepath,run,'\')
path=basepath;
rdfile=strcat(path,'run',lptfile);
imfile1=strcat(path,lptima1);
imfile2=strcat(path,lptima2);

% read data file into header and tensor arrays
fprintf(' Reading single tensor file %s in %s\n',lptfile,path)

fid=fopen(rdfile,'r');
header=fread(fid,64,'int16');
  version=header(1);                % walpt version number (starting with 300)
  nxc =header( 2) ; nyc =header( 3); % camera size
  nxuv=header( 4) ; nyuv=header( 5); % velocity array size
  nxw =header( 6) ; nyw =header( 7); % window sizes in pixels
  nxs =header( 8) ; nys =header( 9); % step sizes in pixels
  nxf =header(10) ; nyf =header(11); % flow region size in pixels
  xf  =header(12) ; yf  =header(13); % flow region offset in pixels
  nbits=header(14);                 % pixel depth of original flow images
  % utensor=[nxuv,nyuv,7]
```

```
  % read tensor components from file in succession
  e1=fread(fid,[nxuv,nyuv],'float'); % u
  e2=fread(fid,[nxuv,nyuv],'float'); % v
  e3=fread(fid,[nxuv,nyuv],'float'); % du/dx
  e4=fread(fid,[nxuv,nyuv],'float'); % dv/dx
  e5=fread(fid,[nxuv,nyuv],'float'); % du/dy
  e6=fread(fid,[nxuv,nyuv],'float'); % dv/dy
  e7=fread(fid,[nxuv,nyuv],'float'); % correlation
st=fclose(fid);

%rotate fields
e1=e1.';
e2=e2.';
e3=e3.';
e4=e4.';
e5=e5.';
e6=e6.';
e7=e7.';

% add (subtract) v_infinity to the velocity field to change
% reference frames to object's frame for tow-tank
% runs.  Set u_infinity to zero to run in lab frame.

for i=1:nyuv
   for j=1:nxuv
      if e1(i,j)<=999
         e1(i,j)=e1(i,j)-u_infinity;
      end
   end
end

for i=1:nyuv
   for j=1:nxuv
```

```
      if e2(i,j)<=999
         e2(i,j)=e2(i,j)+v_infinity;
      end
   end
end

% Check and replace the "missing" 1000 in velocity
% fields with zeros (option XXXX in walpt).
% (This option is for use with IDL or similar programs.)

for i=1:nyuv
   for j=1:nxuv
   if e1(i,j) > 999
         e1(i,j) = 0;
         end
         if e2(i,j) > 999
            e2(i,j) = 0;
         end
    end
end

%Items to return
corr=e7;

% Calculate vorticity,continuity

vorticity=e5-e4;    %du/dy-dv/dx
continuity=e3+e6;   %du/dx+dv/dy

%return velocity gradient for wall skin friction calculation
%(in this case, dv/dx)

dvdx=e4;
```

```
dudy=e5;
return;

function [xsize,ysize]=arraychecker(run,set,batch,basepath)
% MATLAB Script to read WALPT data and image files.
% Jamey Jacob, Jan. 18 2000
% Version 1.1, last modified Feb. 15, 2000
% Miner version May 30, 2001 - only data read
% For use with MATALB release 11 (5.3)
% Ticker will not work with older versions (see "movie")
% jdjacob@uky.edu

% setflag=set;
% set=int2str(set);
run=int2str(run);
bat=int2str(batch);

%run='2b11';

% file and path names
%run='8';lptfile=strcat('tensor',run,'.out');
lptima1=strcat('image',run,'a.lpt');
lptima2=strcat('image',run,'b.lpt');
if batch == 0,
    if setflag == 0
        lptfile=strcat('ten',run,'.out');
    else
    lptfile=strcat('ten',run,'-',set,'.out');
    end
u_infinity=0;
v_infinity=0;
   details=''
else
```

```
if batch < 10
  bat=strcat('.00',bat);
else
if batch < 100
    bat=strcat('.0',bat);
else
  bat=strcat('.',bat);
      end
   end

%    if setflag == 0
       lptfile=strcat(run,bat);
%    else
%      lptfile=strcat(run,'_',set,bat);
%     end
    lptfile=strcat(run,bat);
    lptima1=strcat('image1.lpt');lptima2=strcat('image2.lpt');
     u_infinity=0;
 v_infinity=0;
end

%SET PATHS AND FILE NAMES
%path=strcat(basepath,run,'\')
path=basepath;
rdfile=strcat(path,'run',lptfile)
imfile1=strcat(path,lptima1);
imfile2=strcat(path,lptima2);

% read data file into header and tensor arrays

fprintf(' Checking array size from tensor file %s in %s\n',lptfile,path)

fid=fopen(rdfile,'r');
```

```
header=fread(fid,64,'int16');
  version=header(1);                % walpt version number (starting with 300)
  nxc =header( 2) ; nyc =header( 3); % camera size
  nxuv=header( 4) ; nyuv=header( 5); % velocity array size
  nxw =header( 6) ; nyw =header( 7); % window sizes in pixels
  nxs =header( 8) ; nys =header( 9); % step sizes in pixels
  nxf =header(10) ; nyf =header(11); % flow region size in pixels
  xf  =header(12) ; yf  =header(13); % flow region offset in pixels
  nbits=header(14) ;                % pixel depth of original flow images
  % utensor=[nxuv,nyuv,7]
  % read tensor components from file in succession
  e1=fread(fid,[nxuv,nyuv],'float'); % u
  e2=fread(fid,[nxuv,nyuv],'float'); % v
  e3=fread(fid,[nxuv,nyuv],'float'); % du/dx
  e4=fread(fid,[nxuv,nyuv],'float'); % dv/dx
  e5=fread(fid,[nxuv,nyuv],'float'); % du/dy
  e6=fread(fid,[nxuv,nyuv],'float'); % dv/dy
  e7=fread(fid,[nxuv,nyuv],'float'); % correlation

st=fclose(fid);
xsize=nyuv; ysize=nxuv;
return;
```

Appendix B

Sample WaLPT Input File

```
lptmode, 0=singlepass, 1=small to large, 2=large to small, 3= LPT
2 1 0 1
input file names ( one line per file )
piv8.lst
piv8
image size nxc, nyc, pixr
1008 1018 10 1.00
flow size, nxf, nyf
1008 1018
flow offset, xf, yf
0 0
window size, nxw, nyw, 2**n
32 32
amod, min, max windows dimensions 2**n, correlaltion level corlvl
1 8  32 0.50
step size, nxs, nys
16 16
window type, wtype 1-7, see source listing
1
peak type, ptype 0=grid,1=parabolic,2=gaussian
2
laundary type, ltype 0=no laundering,1=rejection
```

```
0
extension parameter, 0= none, zero padding, 1= smooth (nth order)
1
filter widths (1/) fltrwx,fltrwy; 0= no filtering, 1,2,.. higher ; nfil
10 10 3
wall parameters: nwalls, parex, motion, intflag, outmask
0 0 0 0 0
wall geometry file
junk
motion parameters: dxcg, dycg ,rot
0.00 0.00 0.00
0.00 0.00 0.00
0.00 0.00 0.00
```

References

Adrian, R. J., 1996, "Stratagies for Imaging Flow Fields with Particle Image Velocimetry," *Proceedings*: 27th AIAA Fluid Dynamics Conference, New Orleans, Louisiana, pp. 261-301

Brown, J., 2003, Private communication.

Clouse, B. E., 1982, "Assess Feasibility of Machine Mounted Scrubber System for Ventilation Coal Mine Working Face. Phase I, Interim Report," Ingersoll Rand Research Co., New Jersey.

Divers, E. F., Jayaraman, N. I., Custer, J., 1982, "Evaluation of a Combined Face Ventilation System used with a Remotely Operated Mining Machine, US. Department of Interior, Bureau of Mines, IC 8899. NTIS No. PB 265-934.

Gillies, A. D. S., 1982, "Improved Coal Face Ventilation through Use of Dust Scrubber Systems leads to Greater Production Efficiency," *Proceedings*: First Mine Ventilation Symposium, Tuscaloosa, AL.

Goodman, G. V. R., Taylor, C. D., and Divers, E. D., 1990, "Ventilation Schemes Permit Deep Advance," Coal, October.

Grant, I., 1994, "Selected Papers on Particle Image Velocimetry," SPIE Milestone Series MS 99, SPIE Optical Engineering Press.

Kirkpatrick, A. T., Kenyon A. E., 1998, "Flow Characteristics of Three-Dimensional Wall Jets," *ASHRAE Transactions*, Vol.104, Part 1.

Luxner, J. V., 1969, "Face Ventilation in Underground Bituminous Coal Mines," Bureau of Mines RI 7223.

Raffel, M., Willert, C., and Kompenhans, J., 1998, "Particle Image Velocimetry," a Practical Guide, Springer.

Sholl, M. J., Savas, O., 1997, "A Fast Lagrangian PIV Method for Study of General High Gradient Flows," *35th Aerospace Meeting Exhibits*, AIAA, Paper 97-0493, Reno, Nevada.

Taylor, C. D., Goodman, G. V. R., and Vincze, T., 1992, "Extended Cut Face Ventilation for Remotely Controlled and Automated Mining Systems," Preprints of SME Annual Meeting, Phoenix, AZ.

Taylor, C. D., Rider, J. P., and Thimons, E. D., 1996, "Impact of Unbalanced Intake and Scrubber Flows on Face Methane Concentrations," *Proceedings*: Sixth International Mine Ventilation Congress, Pittsburgh, PA. pp. 169-172

Thimons, E. D., Taylor, C. D., and Zimmer, A., 1999, "Ventilating the Box Cut of a Two-Pass 40-ft Extended Cut," *Proceedings*: Eight US Mine Ventilation Symposium, Kingston, Canada, Vol. 52, No. 3, pp. 108-115

Wala, A. M., Jacob, J. D., Brown, J., and Huang, G., 2003, "New Approaches to Mine Face Ventilation," Mining Engineering, No.3, March, pp. 25-30

Wala, A. M., Jacob, J. D., Huang, G., Brown, J., and Rangubhotla, L., 2004, "How Scrubbers Help Ventilate the Face During Deep Cut Mining with a Blowing Curtain," , March, pp. 307-314

Wala, A. M., Jacob, J. D., and Turner, D., 2002, "Experimental Study of Mine Face Ventilation System for Validation of Numerical Models," *Proceedings*: Ninth U.S. Mine Ventilation Symposium, Kingston, Canada, June, pp. 191-196

Wala, A. M., Jacob, J. D., and Turner, D., 2002, "Particle Image Velocimetry (PIV) used for Mine Face Ventilation Study," *Proceedings*: Ninth U.S. Mine Ventilation Symposium, Kingston, Canada, June, pp. 183-189

Wala, A. M., Stoltz J. R., and Jacob, J. D., 2001, "Numerical and Experimental Study of a Mine Face Ventilation System for CFD Code Validation," *Proceedings*: Seventh International Mine Ventilation Congress, Krakow, Poland. pp. 411-417

Wala, A. M., Stoltz J. R., and Hassan, M. I., 2000, "Scale Modeling of a Mine Face Ventilation System for CFD Code Validation," *Proceedings*: Third International Symposium on Scale Modeling, Nagoya, Japan.

Wellman, T. S., 1981, "Deep Cut Remote Control Mining," Mining Congress Journal, October, Vol. 67, No. 10, pp. 27-30

Vita

Lavanya Rangubhotla was born in Hyderabad, India in 1979. She graduated from St. Theresa's Girls High School, Hyderabad, India in 1995 and received her B-Tech in Mechanical Engineering from Jawaharlal Nehru Technological University in the College of Engineering in 2001. As a graduate student, she worked as a Research Assistant. She presented several talks and papers on her research and is a member of American Institute of Aeronautics and Astronautics. She is currently working as a Senior Associate Engineer in Caterpillar, Inc., Peoria, Illinois.